

THE PROPERTIES OF POOR GROUPS OF GALAXIES: III. THE GALAXY LUMINOSITY FUNCTION

Ann I. Zabludoff¹

UCO/Lick Observatory and Board of Astronomy and Astrophysics,

University of California at Santa Cruz, Santa Cruz, CA 95064

aiz@ucolick.org

and

John S. Mulchaey

The Observatories of the Carnegie Institution of Washington,

813 Santa Barbara St., Pasadena, CA 91101

mulchaey@pegasus.ociw.edu

Accepted for publication in *The Astrophysical Journal*

ABSTRACT

The form of the galaxy luminosity function (GLF) in poor groups — regions of intermediate galaxy density that are common environments for galaxies — is not well understood. Multi-object spectroscopy and wide-field CCD imaging now allow us to measure the GLF of bound group members directly (*i.e.*, without statistical background subtraction) and to compare the group GLF with the GLF's of the field and of rich clusters. We use R-band images in 1.5×1.5 degree² mosaics to obtain photometry for galaxies in the fields of six nearby ($2800 < cz < 7700$ km s⁻¹) poor groups for which we have extensive spectroscopic data (Zabludoff & Mulchaey 1998), including 328 new galaxy velocities (this paper). For the five groups with luminous X-ray halos, the composite group GLF for group members with $-23 + 5\log h < M_R < -16 + 5\log h$ and within projected radii of $\lesssim 0.4 - 0.6h^{-1}$ Mpc from the group center is fit adequately by a Schechter function with $M_R^* = -21.6 \pm 0.4 + 5\log h$ and $\alpha = -1.3 \pm 0.1$.

We also find that (1) the ratio of dwarfs ($-17 + 5\log h \geq M_R > -19 + 5\log h$) to giants ($M_R \leq -19 + 5\log h$) is significantly larger for the five groups with luminous X-ray halos than for the one marginally X-ray detected group, (2) the composite GLF for the luminous X-ray groups is consistent in shape with two measures of the composite R-band GLF for rich clusters (Trentham; Driver *et al.*) and flatter at the faint end than another ($\alpha \approx -1.5$, Smith *et al.*), (3) the composite group GLF rises more steeply at the faint end than the R-band GLF of the Las Campanas Redshift Survey (LCRS; $\alpha = -0.7$ from Lin *et al.*), a large volume survey dominated by

¹New Address: University of Arizona, Steward Observatory, Tucson, AZ 85721, E-mail: azabludoff@as.arizona.edu

galaxies in environments more rarefied than luminous X-ray groups, (4) the shape difference between the LCRS field and composite group GLF’s results mostly from the population of non-emission line galaxies ($\text{EW [OII]} < 5 \text{ \AA}$), whose dwarf-to-giant ratio is larger in the denser group environment than in the field (cf. Ferguson & Sandage, Bromley *et al.*), and (5) the non-emission line dwarfs are more concentrated about the group center than the non-emission line giants, except for the central, brightest ($M_R < M_R^*$) group elliptical (BGG). This last result indicates that the dwarfs, giants, and BGG occupy different orbits (*i.e.*, have not mixed completely) and suggests that some of the populations formed at a different times.

Our results show that the shape of the GLF varies with environment and that this variation is due primarily to an increase in the dwarf-to-giant ratio of quiescent galaxies in higher density regions, at least up to the densities characteristic of X-ray luminous poor groups. This behavior suggests that, in some environments, dwarfs are more biased than giants with respect to dark matter. This trend conflicts with the prediction of standard biased galaxy formation models.

Subject headings: galaxies: luminosity function — galaxies: evolution — galaxies: clusters: general — cosmology: large-scale structure of Universe

1. Introduction

The shape of the galaxy luminosity function (GLF) in a given environment is determined by the initial distribution of galaxy luminosities and by the subsequent galaxy luminosity and number density evolution. Both the initial luminosity and the luminosity/density evolution may depend on environment, causing a variation in dwarf-to-giant ratio (D/G) with environment. For example, the standard model of biased galaxy formation predicts that giant galaxies are more likely than dwarfs to form in regions of high mass density (cf. White *et al.* 1987). After galaxy formation, D/G may be altered by mechanisms whose efficiency is strongly environment-dependent, *e.g.*, galaxy-galaxy mergers are probably more frequent and global tidal fields weaker in poor groups than in rich clusters of galaxies (cf. Zabludoff & Mulchaey 1998, hereafter ZM98). A new class of cosmological models involving “locally biased” galaxy formation (cf. Kauffmann *et al.* 1997; Narayanan *et al.* 1998; Kravtsov & Klypin 1999) has been introduced to modify standard biased galaxy formation and to account for more complex environmental effects on galaxy evolution. Despite some recent progress, observational uncertainties have prevented the behavior of the GLF with environment from becoming a useful constraint.

Most observational determinations of the GLF to date have focused on the field and rich clusters. The GLF is even more uncertain in regions of intermediate galaxy density, like poor groups, that are common galaxy environments. To better constrain the models, and thus the relative effects of environment-dependent galaxy formation and environment-driven galaxy evolution, we must ascertain (1) whether the GLF of poor groups is universal, (2) whether the group GLF differs from the GLF’s of rich clusters and the field, (3) what galaxy populations are most responsible for any environmental differences (*e.g.*, star forming or quiescent galaxies), and (4) whether the GLF varies with local environment within a group itself.

Past determinations of the shape of the poor group GLF differ widely. Some composite group GLF’s are consistent with the field GLF (Muriel *et al.* 1998; Zepf *et al.* 1997), and others suggest a relative depletion of faint galaxies (as reviewed by Hickson 1997) or a dip in galaxy counts at $M_R \sim -18 + 5 \log h$ (Hunsberger *et al.* 1998). Some of the uncertainty arises because the number of known members per group is often small: bound groups cannot be distinguished from chance superpositions of galaxies along the line-of-sight, and the GLF cannot be calculated without statistical background subtraction, a procedure sensitive to inhomogeneities in the large-scale structure (especially for low surface density contrast groups). Furthermore, it is difficult to compare existing group GLF’s with those of the field and rich clusters, because previous studies focus almost exclusively on Hickson Compact Groups (HCG’s; Hickson 1982), which are defined by their unusually concentrated bright galaxy population and thus represent only one subset of groups in general.

The first step in addressing these problems is to identify a sample of poor groups

with (1) the properties of bound systems, *i.e.*, where there is evidence that members lie in a common potential well, (2) a large number of spectroscopically-confirmed members in each system, and (3) galaxy environments different than those explored in past work. In ZM98a and MZ98, we found that poor groups with luminous, extended X-ray halos also have significant dwarf populations and that global X-ray properties such as luminosity and temperature are well-correlated with global optical properties like galaxy velocity dispersion. These results argue that the members of an X-ray luminous group are bound.

The large number of known members (~ 30 -60) in each X-ray group not only renders background subtraction unnecessary, but also makes statistically significant comparisons possible. In particular, we can learn whether this class of bound groups has a common GLF, and, if not, what galaxy populations are responsible for the differences. Furthermore, we can test whether the spatial distributions of distinct galaxy populations *within* groups are consistent with any global, density-dependent trends observed when comparing GLF's of the field, poor groups, and rich clusters.

The shape of the GLF for members of poor, X-ray luminous groups also provides insight into galaxy evolution in an environment that has not been isolated previously. Field studies such as the Las Campanas Redshift Survey (LCRS; Lin *et al.* 1996) are dominated by galaxies in even more rarefied environments than X-ray luminous groups (*i.e.*, by members of poorer groups and by galaxies outside of associations). Many HCG's and other optically-selected poor group candidates do not have a hot, extended intragroup medium. In contrast, some properties of X-ray luminous groups are consistent with an extrapolation of rich cluster properties to lower masses (MZ98; ZM98b). A direct comparison of the GLF's for these groups, rich clusters, and the field has yet to be made.

In this paper, we combine multi-object spectroscopy and wide-field CCD imaging of a sample of five nearby, X-ray luminous poor groups, including three non-HCG's, to determine the form of the group GLF. For comparison, we also discuss the properties of a sixth group, NGC 3557, that is marginally X-ray-detected. We describe the group sample, the photometry, and the spectroscopy in Section 2. Section 3 contains the GLF determinations for individual groups, a comparison of the composite GLF for the five X-ray luminous groups with the GLF's for rich clusters and the field, an analysis of the relative contributions of star forming and quiescent galaxies to the differences between the group and field GLF's, and a comparison of the spatial distributions of dwarf and giant group members. Section 4 reviews some of the implications of our results for models of galaxy formation and evolution. Our conclusions are summarized in Section 5.

2. The Observations

2.1. The Group Sample

A poor group is defined optically as an apparent system of fewer than five bright ($\lesssim M_R^*$) galaxies. To isolate the form of the GLF in poor groups with luminous X-ray halos, we examine five X-ray-detected poor groups originally discussed in ZM98. All five groups have extended ($> 100 \text{ h}^{-1} \text{ kpc}$), luminous ($L_X \sim 10^{42} \text{ h}^{-2} \text{ erg s}^{-1}$) X-ray emission imaged by the ROSAT Position Sensitive Proportional Counter (PSPC) (Mulchaey & Zabludoff 1998; hereafter MZ98). For comparison, we obtain galaxy spectroscopy and photometry for a sixth group, NGC 3557, that is marginally-detected by ROSAT ($L_X = 2.8 \times 10^{40} \text{ h}^{-2} \text{ erg s}^{-1}$) and that has an asymmetric, unrelaxed X-ray morphology (Figure 1). The X-ray temperature of NGC 3557 is also significantly lower ($\sim 0.5 \text{ keV}$), than is typical for the X-ray luminous groups ($\sim 1 \text{ keV}$), although NGC 3557’s temperature is poorly constrained due to the group’s relatively low X-ray luminosity. Because NGC 3557 extends over an optical radius comparable to that of the other groups, its lower temperature implies a lower mass density. This argument is supported by NGC 3557’s relatively low galaxy number density and velocity dispersion (cf. Table 2). The six groups have mean velocities of $2800 < cz < 7700 \text{ km s}^{-1}$, virial masses of $\sim 10^{13} - 10^{14} M_\odot$, and a brightest group galaxy (BGG) that is a giant elliptical located in the group center (cf. ZM98a).

2.2. Spectroscopic Data

We obtained spectra for 742 galaxies in the six sample groups with the multi-fiber spectrograph (Schechter *et al.* 1992) and 2D-Frutti detector mounted on the du Pont 2.5m telescope at the Las Campanas Observatory. Of these spectra, 328 are new observations, and the remainder are from ZM98. To define galaxy targets in each group field over the $1.5 \times 1.5 \text{ degree}^2$ field of the fiber spectrograph, we used coordinates, star/galaxy classifications, and relative magnitudes from FOCAS (Jarvis & Tyson 1981) and the STScI Digitized Sky Survey. The uncalibrated, relative magnitudes drawn from the plate scans were sufficient to identify the ~ 200 brightest galaxies in each field. For each group, we observed 1-3 fiber fields, starting with the brightest galaxies. The completeness of the spectroscopic sampling of each group field as a function of galaxy magnitude is discussed in the next section and in §3.1.

We determine radial velocities from the spectra using the cross-correlation routine XCSAO and the emission line finding routine EMSAO in the RVSAO package in IRAF (Mink & Wyatt 1995). The velocities in Table 1 are either emission line velocities, absorption line velocities, or a weighted average of the two (see Schechter *et al.* 1997 (their §2.2) or Lin 1995 for a discussion of the cross-correlation templates and the spectral lines typically observed). We compute velocity corrections to the heliocentric reference frame with the IRAF/HELIO program. See ZM98 for a discussion of the

velocity zero-point correction and external velocity error determinations.

The distribution of galaxy velocities, the total number of galaxies with velocities (N_{tot}), and the number of group members (N_{grp}) in each of the six fields are shown in Figure 2.

2.3. Photometric Data

We acquired images for the six groups under photometric conditions using the 40-inch telescope at Las Campanas Observatory during October 1996 and February 1997. The detector was a Tektronics 2048² CCD with a field of view of $\sim 23.8'$ on a side. To cover the entire 1.5×1.5 degree² area of our fiber spectroscopy field, we obtained a 5×5 mosaic in all cases except for the more distant NGC 4325 group, for which a 3×3 mosaic was sufficient to image nearly all of the spectroscopically-confirmed group members. Each tile of the mosaic has a $\sim 5'$ overlap with an adjacent tile.

The total exposure time for each tile is 5 minutes with a Kron-Cousins R filter from the Harris set. The typical seeing was $\sim 1.5''$. We reduce the images using standard techniques in IRAF. The bias level is determined from the overscan region of the CCD and subtracted from the images. Flat-fielding is accomplished using dome flats. The images are flux-calibrated using standard star fields in Graham (1982).

Once the images are calibrated, we use the program SExtractor (Bertin & Arnouts 1996) to classify objects as stars or galaxies and to measure total magnitudes. For the purposes of this study, we consider all objects with a “stellarity-index” of less than 0.5 as galaxies. To verify that this classification is valid, we examine plots of isophotal surface area versus magnitude for each field. These plots indicate that the star/galaxy separation is typically valid down to $m_R \approx 19.5 - 20$. However, a small fraction of the images (less than 10%) were taken under poor seeing conditions ($\sim 2.5''$). In these cases, the star/galaxy separation is less robust. To quantify the success of the SExtractor classification for these fields, we visually classify the objects in one group, HCG 62. We find that the SExtractor classification is consistent with our visual classification for all objects brighter than $m_R = 18$. In the range $18 < m_R < 19$, the two methods yield consistent results 85% of the time.

In most cases, total magnitudes are measured using a method similar to that proposed by Kron (1980). However, the Kron method relies on aperture magnitudes, which are sensitive to crowding in the field. Thus, if a galaxy has nearby neighbors, the Kron magnitude may be inaccurate. A better estimate of the true magnitude in these cases is a corrected isophotal magnitude (see discussion in the SExtractor manual). Therefore, we adopt the ‘MAG.BEST’ option in SExtractor, which computes a corrected isophotal magnitude when crowding is a problem and a Kron magnitude otherwise. For the six group fields, the Kron method is used to calculate the total magnitude in more than 80% of the galaxies.

We estimate the errors in the ‘MAG_BEST’ R magnitudes obtained from SExtractor in several ways. Because the CCD mosaic tiles overlap, about 30% of the galaxies are imaged more than once. From these multiple measurements, we estimate that the typical internal magnitude errors are about 0.05 mag. These errors are consistent with the median of those output by SExtractor for galaxies brighter than about $m_R = 17$. A few of the galaxies have previously measured total magnitudes in the R band listed in the NED database. A comparison of these magnitudes with our data yields a median external error estimate of about 0.15 mag. While total R magnitudes only exist for a handful of our targets, many others have R-band aperture measurements in the literature. A comparison of our photometry with that in the literature in the same size aperture is consistent with our external error estimate derived from the comparison of total magnitudes.

The completeness of the spectroscopic survey of each group field is shown in Figure 3. For each m_R bin, we indicate the fractional completeness of the spectroscopic data relative to the photometric catalog of SExtractor-identified galaxies. In the case of NGC 4325 and of NGC 5129, there are two distributions of m_R — one for the entire spectroscopic/photometric catalog and the other sampled within a smaller radius of $0.6h^{-1}$ to make it consistent with the sampling radii ($\sim 0.4 - 0.6h^{-1}$ Mpc) for the other groups. Note that we use the smaller radius sample for all subsequent analyses involving NGC 4325 and NGC 5129.

As a complement to this paper, we have submitted a table of the galaxies in each group field with measured velocities to the NASA/IPAC Extra-galactic Database ((NED), Helou *et al.* 1991). This table contains the galaxy name, J2000 coordinates, heliocentric velocity and error, type of velocity measurement (*i.e.*, from absorption lines “0”, emission lines “1”, or a combination of both “2”), and R-band total magnitude for the 742 galaxies with measured velocities. Table 1 shows an example of the format. The full table is also available in electronic form from the authors on request.

Table 2 summarizes the properties of the six sample groups, listing the group name, projected centroid calculated from the coordinates of the group members in J2000 (unweighted by galaxy luminosity), number of members (N_{grp}), mean heliocentric velocity (\bar{v}), line-of-sight velocity dispersion (σ_r), total X-ray luminosity (L_X), sampling radius for the photometry (r_{samp} ; same as in Figure 4), number of members within r_{samp} (N'_{grp}), corrected number density of galaxies with $M_R \leq -17 + 5\log h$, within $0.4h^{-1}$ Mpc of the group center, and assuming spherical symmetry ($n_{0.4}$), and dwarf-to-giant ratio for galaxies with $M_R \leq -17 + 5\log h$ and within $0.4h^{-1}$ Mpc ($D/G_{0.4}$; defined as in §3.1).

3. Results

3.1. Individual Group GLF's

Is the GLF universal among poor groups of galaxies? For a sample consisting of five groups and the Virgo and Fornax clusters, Ferguson and Sandage (1991) argue that the early type dwarf-to-giant ratio increases with the richness of the system. However, as discussed by those authors, the interpretation of their results is complicated by the lack of spectroscopic data and inhomogeneities in the radial sampling of the group and cluster images. With spectroscopic surveys of galaxies in the fields of poor groups (ZM98a; MZ98; this paper), we can ascertain more directly which groups are likely to be bound systems instead of chance superpositions and which galaxies are group members instead of interlopers.

Our earlier work suggests significant differences in D/G as a function of local mass density — although the number of giant group members is comparable, groups that are X-ray detected have higher velocity dispersions (200-450 km s⁻¹ vs. < 200 km s⁻¹) and larger memberships (20-50 galaxies vs. < 10 galaxies) than non-X-ray-detected groups (also see Hunsberger *et al.* 1998). Unfortunately, the small number of members in the non-X-ray groups prevents us from determining if they are bound. Therefore, to test whether D/G does vary with mass density, we compare the individual group GLF's for a sample of six X-ray-detected groups, including N3557, a marginal detection and lower mass density environment.

The distribution of galaxy luminosities for each group is shown in Figure 4. The absolute magnitudes are calculated for a $H_0 = 100$ km s⁻¹ Mpc⁻¹, $q_0 = 0.5$ cosmology. For each group, we apply a global extinction correction of $A_R = 0.58A_B$, where A_B is the extinction in the B-band at the group's center (NED) and the conversion factor is estimated from the extinction curve of Schild (1977). The GLF's are also corrected for incompleteness (see Figure 3) by assuming that, within each magnitude bin, the fraction of galaxies without velocities that are group members is the same as the fraction of measured galaxies that are members. Down to $M_R \leq -17 + 5\log h$, the faint limit of our subsequent analyses, the completeness corrections are small for each group (*i.e.*, the corrected and uncorrected counts are consistent within the 1σ counting errors). Note also that for these completeness corrections, HCG 42, HCG 62, and NGC 3557 are $\gtrsim 50\%$ complete within the $-17 < M_R \leq -16 + 5\log h$ bin.

To test whether the distributions of galaxy luminosities differ among the groups, we calculate a dwarf-to-giant ratio, D/G . We define giants as galaxies with $M_R \leq -19 + 5\log h$ (corresponding to $\lesssim M_R^* + 2.5$) and dwarfs by the range $-17 + 5\log h \leq M_R < -19 + 5\log h$ (corresponding roughly to $M_R^* + 2.5$ to $M_R^* + 4.5$, our faint end completeness limit; §3.2)². To ensure that D/G is calculated uniformly for all the

²Note that unlike Ferguson & Sandage (1991), who used galaxy surface brightness to both assign group membership and to separate early type dwarfs from giants, we separate the dwarf and giants samples by galaxy luminosity. Another

groups, we consider only members within $0.4h^{-1}$ Mpc of each projected group center and completeness-correct the counts ($D/G_{0.4}$; see Table 2).

We calculate the errors in $D/G_{0.4}$ by assuming Gaussian counting statistics (which are indistinguishable from the true Poisson errors for all but the brightest bins in Figure 4). The errors for the completeness-corrected counts are determined with standard error propagation. The assumption of counting errors does not reflect an intrinsic uncertainty in the number of galaxies in any magnitude bin (for $M_R < -17 + 5\log h$, the bins are complete or nearly so and the only source of error is magnitude uncertainties). Instead, the errors provide estimates of how well the individual group GLF determines the universal GLF (if it exists). Because these errors assume that all groups are drawn from the same parent GLF, they are useful in testing whether the group $D/G_{0.4}$ ’s are statistically different from one another.

The $D/G_{0.4}$ values for the five groups with X-ray luminous halos are not statistically different. However, the relative dearth of $-20 + 5\log h \geq M_R > -17 + 5\log h$ galaxies in the galaxy luminosity distribution of NGC 3557 compared with the X-ray luminous groups produces a lower $D/G_{0.4}$. The composite $D/G_{0.4}$ of the five X-ray luminous groups (computed by normalizing each group’s GLF to that of HCG 42 and averaging; see §3.2) is 1.9 ± 0.4 , which differs at the $> 4\sigma$ level from NCG 3557’s value of 0.2 ± 0.2 . For comparison, the Local Group’s D/G is roughly < 0.8 in this magnitude range (Grebel 1999).

Although $D/G_{0.4}$ is lower in the NGC 3557 group than in the other groups down to our completeness limit of $M_R < -17 + 5\log h$, NGC 3557’s galaxy luminosity distribution rises at fainter magnitudes (even the uncorrected, lower-limit counts rise). Deeper spectroscopic surveys of the other, more distant groups will determine whether the behavior of their extreme faint end GLF’s is similar to that of NGC 3557. The “dip” in NGC 3557’s GLF is roughly consistent in shape with the composite GLF for mostly non-X-ray luminous Hickson Compact Groups observed by Hunsberger *et al.* 1998, who suggest that dynamical friction and galaxy mergers cause intermediate luminosity galaxies to acquire mass and to move to the bright end of the GLF in some poor groups. The low specific globular cluster frequency and high rotational velocity of NGC 3557 itself are consistent with a merger product (van den Bergh 1986). Additional explanations for differences among the GLF’s of groups are discussed in §4.

The results of this section suggest that the GLF is not universal among poor groups and that D/G may increase with the mass density of the group environment. In the next section, we examine whether this trend in D/G continues from the field to poor groups to rich clusters.

difference is that the faint end limits of our survey are typically > 1.5 magnitudes brighter.

3.2. Composite Group GLF

Because luminous, extended X-ray emission suggests a common potential well and is roughly correlated with the number density of group galaxies, the fraction of early type members, and the group velocity dispersion (ZM98; MZ98), a sample of X-ray luminous groups is likely to contain a higher fraction of bound systems than a sample of group candidates identified only as galaxy concentrations in velocity space and on the sky. As a result, determining the GLF for X-ray luminous groups is an important first step in isolating the effects of group environment on the evolution of galaxies. With our sample, it is now possible to compare the shape of the GLF in three *distinct* environments: the Las Campanas Redshift Survey of the field, X-ray luminous groups, and rich clusters of galaxies.

We construct a composite GLF from the five groups with luminous X-ray halos by arbitrarily normalizing each to have the same number of completeness-corrected galaxy counts brighter than $M_R = -17 + 5\log h$ as HCG 42. We then average the five individual, completeness-corrected group GLF's. This procedure ensures that the shape of the composite GLF is not weighted more by groups like HCG 62 and NGC 2563, which have relatively high galaxy densities. Because HCG 42 and HCG 62 are complete to within a factor of two for galaxies with $-17 + 5\log h \geq M_R \geq -16 + 5\log h$, we average the corrected galaxy counts for these two groups only to obtain the composite point for that bin. However, only the five bins brighter than $M_R = -17 + 5\log h$ are used in subsequent determinations of D/G .

The composite GLF for group members with $-23 + 5\log h < M_R < -16 + 5\log h$ and within projected radii of $\lesssim 0.4 - 0.6h^{-1}$ Mpc from the group center is consistent with a Schechter function of form $M_R^* = -21.6 \pm 0.4 + 5\log h$ and $\alpha = -1.3 \pm 0.1$ (Figure 5). Figure 5 also shows two composite GLF's for rich clusters (Trentham 1997 (includes Coma), Driver *et al.* 1998) and the GLF for the Las Campanas Redshift Survey (hereafter LCRS) of the field (Lin *et al.* 1996). The field and cluster GLF's are normalized so that the number of galaxies brighter than $M_R < -17 + 5\log h$, roughly the completeness limit for the group and LCRS samples, is the same as for the group composite. The completeness of the cluster samples, as derived from background-subtracted, not spectroscopic, counts, is estimated to be one or two magnitudes fainter. The two cluster GLF's, which are calculated from different cluster samples, are consistent with one another within the errors except in the $M_R = -21.5 + 5\log h$ bin. The cluster galaxies in this bin contribute little ($\sim 2\%$ for Trentham, $\sim 12\%$ for Driver *et al.*) to the total number of giants with $M_R < -19 + 5\log h$, and thus the D/G 's of the two cluster samples are similar.

Although we have measured most or all of the group members brighter than $M_R < -17 + 5\log h$ in each group, the statistics of the group sample are not adequate to distinguish among different functional forms for the composite GLF (*e.g.*, between the single Schechter function and a two-component fit (cf. Hunsberger *et al.* 1998).

Over this magnitude range, the cluster and LCRS GLF’s are also well fit by single Schechter functions, and the composite group data, not the fit, are compared to these GLF’s in the next two sections. Even the addition of NGC 3557, whose GLF suggests a non-Schechter functional form (cf. Figure 4), does not significantly alter the composite (*i.e.*, the Schechter function is not excluded by a χ^2 fit, and M_R^* and α are within the original 1σ errors).

We stress that the field, group, and cluster GLF’s in Figure 5 do not represent the absolute contribution of each environment to a unified GLF, as the normalizations are arbitrary. Instead, the shape of each GLF suggests the typical luminosity distribution of member galaxies in that environment. To properly normalize the composite group GLF for bound groups over the mass range of our sample ($\sim 10^{13}$ - $10^{14} M_\odot$), we would need to know what fraction of groups cataloged from optical redshift surveys are bound and what fraction of bound groups have luminous X-ray halos, marginal X-ray detections, or non-X-ray-detections.

3.2.1. Comparison with Rich Clusters

How do the GLF’s for poor groups compare with those for rich clusters of galaxies? Determinations of individual cluster GLF’s vary in part due to differences in observed waveband (cf. Wilson *et al.* 1997) and in mean sample redshift, factors that are sensitive to morphology and/or star formation history. However, as in the case of poor groups, there is evidence for intrinsic variations among the GLF’s of rich clusters (cf. López-Cruz *et al.* 1997; Driver *et al.* 1998). To investigate whether there are global trends in the shape of the GLF from poor groups to rich clusters, we compare our R-band composite GLF for X-ray luminous groups with three composites of nearby ($z \leq 0.2$) clusters in the R-band (Trentham 1997, Smith *et al.* 1997, and Driver *et al.* 1998).

Figure 5a shows that our composite GLF and those derived from four rich clusters (Trentham 1997) and from seven other rich clusters (Driver *et al.* 1998) are consistent down to $M_R < -16 + 5\log h$ and also over the extrapolation of the group GLF one magnitude fainter (a χ^2 test is unable to distinguish at the $> 95\%$ confidence level among the three GLF’s over these magnitude ranges). Smith *et al.* derive a somewhat steeper faint end slope from a composite of three rich clusters ($\alpha \approx -1.5$ vs. $\alpha \approx -1.3$). The Trentham and Driver *et al.* GLF’s are constructed from Kron total magnitudes (Smith *et al.* use isophotal magnitudes), which are typically equivalent to the SExtractor ‘MAG_BEST’ magnitudes (§2.3) in our group GLF. All three cluster GLF’s are determined using statistical background subtraction.

In fitting their cluster composite, Smith *et al.* obtain a slightly better fit using two Schechter functions instead of one (both the one- and two-Schechter fits have steeper faint end slopes than Trentham and Driver *et al.* over the magnitude range

of our data). Smith *et al.* include the Coma cluster, which has either a sharp rise that exceeds a single Schechter function at faint magnitudes or an actual dip due to a relative deficit of dwarf galaxies with $M_R \sim -18 + 5 \log h$ (Secker & Harris 1996). The Coma cluster is highly complex, with several recently accreted groups. If some of these infalling groups have GLF’s that are better fit by two components (cf. Hunsberger *et al.* 1998; Koranyi *et al.* 1998), the overall shape of the Coma GLF may be determined in large part by the contributions of those subclusters (cf. Secker & Harris 1996). This suggestion is supported by the consistent dwarf-to-giant ratios of Coma and of the similarly complex, but poorer, Virgo cluster (Thompson & Gregory 1993).

Differences among the GLF’s of individual groups and rich clusters might result from an environment-dependent combination of type specific GLF’s (Binggeli, Sandage, & Tammann 1988; Jerjen & Tammann 1997). It is also possible that two galaxies of the same initial morphology might experience different density and/or luminosity evolution depending on their environment, leading to evolution in the type-specific GLF’s. For example, López-Cruz *et al.* (1997) and Driver *et al.* (1998) find a different trend among clusters than we do among groups and than Thompson & Gregory (1993) and Valotto *et al.* (1997) find among other clusters — namely, that dwarf-to-giant ratio decreases with increasing global projected galaxy density. Driver *et al.* observe the effect only outside the core, a region more sensitive to background subtraction and cluster substructure. However, their result suggests that the trends in D/G among poor groups and from the field to poor groups may be reversed in some rich clusters by a different galaxy evolution history.

While the details of the inter-dependence of galaxy type, luminosity, and environment await future surveys, we conclude here that the typical D/G of rich clusters is either consistent with (cf. Trentham 1997, Driver *et al.* 1998) or larger than (cf. Smith *et al.* 1997) that of X-ray luminous poor groups.

3.2.2. Comparison with LCRS Field

Estimates of the luminosity function of galaxies in the nearby ($z \sim 0.1$) field vary as much as the observed GLF’s for rich cluster members. As in the case of the cluster GLF, the uncertainty in the field GLF arises in part from the difficulty in translating the different photometric filters employed by redshift surveys into the same band. Such translations may ignore potentially important effects, including the initial selection of galaxies from different bands, variations in galaxy color with absolute magnitude (*e.g.*, the “mass-metallicity relation”), and intrinsic differences between the dwarf-to-giant ratios of blue and red galaxies (witness the differences between the emission and non-emission line GLF’s discussed in §3.3). It is therefore essential to compare our R-band composite group GLF with a R-band GLF of the field.

Another issue is how fairly a given survey samples the nearby universe. For

example, it is possible that high density environments are overrepresented in the R-band CfA Century survey (Geller *et al.* 1997), which contains portions of the Corona Borealis supercluster and of seven Abell clusters (including Coma). In contrast, the larger, R-band Las Campanas Redshift Survey (LCRS; Shectman *et al.* 1996) is known to be dominated by galaxies in environments more rarefied than X-ray luminous groups. Fully 87% (18590 out of 21343; cf. Tucker *et al.* 1998) of LCRS galaxies lie outside of poor groups or in groups that have lower velocity dispersions ($\leq 200 \text{ km s}^{-1}$), and presumably lower mass densities, than groups in our X-ray sample. Although this fraction may be overestimated relative to the “true” field due to that fiber survey’s tendency to undersample overdense regions, the LCRS is an appropriate choice for comparing our GLF for X-ray luminous, poor group members with that for galaxies in typically less dense environments.

Figure 5b shows the GLF of the composite of the X-ray luminous groups and the best Schechter fit to the LCRS field survey GLF (Lin *et al.* 1996). If the arbitrary LCRS normalization is adjusted to minimize χ^2 with respect to the group GLF for galaxies brighter than the estimated LCRS completeness limit of $M_R = -17.5 + 5\log h$ (Lin *et al.* 1996), the LCRS field GLF is excluded at the $> 95\%$ level. (The best χ^2 normalization is in fact lower than that shown). Relative to the field, poor groups with luminous X-ray halos have either a deficit of giants, an excess of dwarfs, or a combination of both effects.

The difference between the LCRS field and the poor group composite is not due to the difference between the isophotal magnitudes used in the LCRS GLF and SExtractor ‘MAG_BEST’ magnitudes calculated for the group members. From the galaxies in our sample with $10.3 \leq m_R \leq 17.3$ (the magnitude range used to calculate the group GLF), we estimate that the isophotal to ‘MAG_BEST’ magnitude correction to the LCRS GLF is typically $\lesssim -0.2$. This value is consistent with that estimated by Lin *et al.* (-0.35 ± 0.1 ; 1996). Applying this correction, which increases slightly towards fainter magnitudes, only furthers the disagreement between the LCRS field and the composite group GLF’s in Figure 5b.

Incompleteness in the LCRS is unlikely to be the source of the trend towards higher D/G in the denser, group environment. First, we compare the group and LCRS samples only down to the estimated M_R limit above which the LCRS is completeness-corrected (Lin *et al.* 1996)³. Second, the observed increase in D/G with density is consistent with the results of an analysis of the LCRS itself (Bromley *et al.* 1998), where any faint incompleteness in the galaxies would be either uniform across the sample or greater in higher density regions. Third, it is suggestive that the only other large R-band survey of the nearby field (the CfA Century survey, Geller *et al.* 1997) has both a higher average galaxy density and a larger dwarf-to-giant ratio than

³We address the possibility of type-dependent incompleteness in §3.3.

the LCRS ($\alpha = -1.2$ vs. $\alpha = -0.7$, respectively).

In summary, D/G increases from the LCRS field, which is dominated by galaxies in poorer groups and outside of groups, to groups with X-ray luminous halos.

3.3. Star Forming vs. Quiescent GLF's

Is it possible to isolate the galaxy population most responsible for the increase in the D/G between the field and X-ray luminous groups? Ferguson & Sandage (1991) suggest that the differences between the dwarf-to-giant ratios of groups and clusters are due mostly to an increase in the early-type dwarf-to-giant ratio with richness. A recent analysis of the LCRS (Bromley *et al.* 1998) using spectroscopically-defined galaxy morphologies also finds that the early type dwarf-to-giant ratio increases with local density. By analyzing the emission line characteristics of the group and LCRS galaxies, we can divide the data into star forming and non-star forming (quiescent) galaxies. As in Lin *et al.* 1996, we define star forming group members as those with $[\text{OII}] \text{ EW} > 5\text{\AA}$ (approximately the Galactic value). Galaxies with a weaker or non-detectable $[\text{OII}]$ line are classified as quiescent.

The GLF's for the divided samples are shown in Figure 6. For both the LCRS and the group samples, the GLF for star forming galaxies rises more steeply than that for quiescent galaxies. The two GLF's for the LCRS sample are each normalized to have the same number of galaxies brighter than $M_R = -17 + 5\log h$ as the corresponding composite group GLF's.

For the five brightest bins (corresponding roughly to the LCRS completeness limit), the quiescent galaxies in the LCRS field and in the X-ray luminous groups have different GLF's, *i.e.*, adjusting the relative normalizations to minimize χ^2 excludes the field sample at $> 95\%$ confidence. The χ^2 minimization also forces the normalization lower than plotted, increasing the differences between the field and the groups at the faint end. In contrast, the star forming galaxies have roughly consistent GLF's down to the $M_R \sim -17.5 + 5\log h$ bin (the χ^2 minimization test does not distinguish between the two star forming GLF's).

One potential problem in interpreting these results is that noise in a spectrum can be mistaken for an $[\text{OII}]$ emission line. Therefore, in the case of low signal-to-noise spectra (*i.e.*, dwarfs), it is possible to overestimate the number of star forming galaxies. We test the magnitude of this effect by applying an $[\text{OII}]$ flux cut of $> 2\sigma$ to the star forming sample. Although the number of group members classified as star forming is reduced from 48 to 26, and the number of quiescent galaxies is correspondingly increased, the resulting GLF's are consistent with those in Figure 6.

Another consideration is that the mean redshift of the LCRS galaxies is higher than for the group sample ($z \sim 0.1$ vs. 0.017 , respectively). As a result, the fixed $3.5''$ size of the spectroscopic fiber subtends, on average, different physical radii for the LCRS and

group samples. Because of this aperture bias, light is sampled within the inner $\sim 1h^{-1}$ kpc of a group galaxy at the average survey depth, in contrast to the $\sim 4h^{-1}$ kpc sampling typical of LCRS galaxies. However, aperture bias is unlikely to significantly affect the star forming/quiescent galaxy classifications and the disagreement between the group and field GLF’s for the following reasons. The dominant effect of aperture bias would be to prevent the detection of HII regions in the disks of group members, causing some star forming galaxies to be misclassified as quiescent. This problem is rare because the effect is only significant for face-on galaxies (inclined disks tend to have HII regions along the line-of-sight). For example, few emission line spirals are classified as non-emission line galaxies (about 1 of 12 within 15000 km s^{-1} ; Zaritsky, Zabludoff, and Willick 1995). Not only are the effects of aperture bias on the GLF’s (arbitrary) normalization small, but they are unlikely to alter the GLF’s *shape*, the basis of our comparison of the group and field populations.

One way to artificially reproduce the trends in Figure 6 is to stipulate that many faint emission line dwarfs are missing from the LCRS and that environmental conditions in groups convert them to non-emission line dwarfs. However, this model is problematic. First, such a transformation between star forming and quiescent dwarfs is unlikely. Although mechanisms like tidal stripping or “galaxy harassment” (Moore *et al.* 1996; Moore *et al.* 1998) have been proposed for transforming star forming irregulars or Sd’s into quiescent spheroidals, studies of dIrr’s and dE’s in Virgo show that the structures defined by the old stellar populations differ significantly between the two types of dwarfs. For example, the dIrr’s have more flattened and asymmetric stellar light distributions, and no dIrr’s have H-band luminosities or surface brightnesses as high as those of the brightest dE’s (James 1991).

Second, incompleteness in the LCRS does not affect our results significantly. Huchra (1999) argues from the B-band CfA2 redshift survey that the LCRS selection criteria exclude more faint, low surface brightness galaxies than are corrected for by Lin *et al.* (1996) and that these galaxies have mostly emission line spectra. Even if it were simple to compare B-band data directly with the R-band LCRS (and, for the reasons cited earlier, it is not), the following argument suggests that the effects of any missing galaxies are small by showing that the combination of incompleteness and of dwarf transformation leads to consequences that we do not observe.

Is it possible to transform the field GLF into the group GLF by changing field emission line dwarfs into group non-emission line dwarfs? We define the total number of field galaxies at $M_R = -17.5 + 5\log h$ that will become group galaxies as $E_i + N_i$, where E_i and N_i are the number of star forming and quiescent dwarfs, respectively, in the field. The final number of group galaxies in the $M_R = -17.5 + 5\log h$ bin is then $E_f + N_f = E_i + N_i$, where E_f and N_f are the star forming and quiescent group dwarfs, respectively. First, we correct for the “missing” field dwarfs. The difference between the CfA2 and LCRS emission line galaxy counts at $M_R = -17.5 + 5\log h$ is a factor of

~ 4 (Huchra 1999). The difference between the LCRS emission line and non-emission line counts in this bin is a factor of ~ 6 (Lin *et al.* 1996, as opposed to the arbitrary relative normalization shown in Figure 6). If we “correct” the LCRS emission line counts by the CfA2 value, the ratio of emission to non-emission line counts in the field is ~ 24 at $M_R = -17.5 + 5\log h$, *i.e.*, $E_i = 24N_i$. Second, we measure the ratio of group emission to non-emission line dwarfs. Figure 6 shows that $E_f \sim 1/2N_f$. Therefore, $3/2N_f = 25N_i$, and this model predicts that the final ratio of quiescent dwarfs in groups to those in the field would be ~ 17 at $M_R = -17.5 + 5\log h$, while the ratio for giants does not change. This result is at odds with Figure 6, in which only a boost of at most $\sim 5\times$ in the number of quiescent field dwarfs relative to giants is required to match the observed group population. The model, in which many faint emission line dwarfs are missing from the LCRS and are converted by group environment into non-emission line dwarfs, over-predicts the ratio of quiescent group dwarfs to quiescent group giants. Because the model is wrong, the effects of LCRS incompleteness on our results are likely to be small.

In summary, we find in this section that the quiescent D/G in groups is significantly larger than that of the field. This result indicates that quiescent dwarfs are more clustered than quiescent giants, although it is not clear whether an excess of dwarfs, a deficit of giants, or some combination of both effects, is responsible.

3.4. Spatial Distribution of Dwarfs vs. Giants

In previous sections, we find that D/G increases with mass density among groups, that D/G increases from the field to groups (and may continue to increase from groups to clusters), and that a change in the D/G of non-star forming galaxies is the cause of the increase from the field to groups. Therefore, if this trend is real, we might expect D/G to increase *within* groups from the outskirts to the denser core. Such behavior would be opposite to the effect of mass segregation and to the prediction of standard biased galaxy formation. Ferguson & Sandage (1991) identify no radial gradients in the surface brightness-defined dwarf-to-giant ratio in their study of the Virgo, Fornax, and Antlia systems. The luminosity-defined dwarf-to-giant ratio of rich clusters in the Driver *et al.* (1998) sample rises from the inner ($r \leq 0.28h^{-1}$ Mpc) to outer ($0.28 < r \leq 0.37h^{-1}$ Mpc) annulus for some systems and falls for others. Here we test for such gradients in our luminosity-defined D/G .

First we compare the kinematic and spatial distributions of the BGGs, dwarfs, and giants for all six groups (Figure 7ab). Figure 7a is the composite phase space diagram for the 123 quiescent galaxies. The y-axis shows the velocity offset of the galaxy from the mean velocity of the group, the x-axis shows the projected radial offset from the projected group centroid normalized by the group velocity dispersion. The six sample

galaxies with $M_R < M_R^*$ are marked by asterisks and include four BGG's⁴, which are consistent with the kinematic and spatial center of their groups (ZM98a). There is also an apparent concentration of dwarfs (small filled circles) toward the group center relative to giants (large open circles).

To compare the distributions of the samples on the sky and in velocity space simultaneously and quantitatively, we define the statistic $R^2 = (x/\delta_x)^2 + (|y|/\delta_{|y|})^2$, where δ_x and $\delta_{|y|}$ are the *rms* deviations in x and $|y|$ for the entire sample (cf. ZM98). Thus, a galaxy that has a large peculiar motion and/or that lies outside the projected group core will have a larger R value than a galaxy at rest in the center of the group potential. The distributions of R for the four BGGs and two other $M_R < M_R^*$ galaxies (heavily shaded), 56 giants (shaded), and 61 dwarfs (unshaded) are in the right-hand panel. A Kolmogorov-Smirnov test indicates that the dwarf and giant (and the $M_R < M_R^*$ and giant) samples differ from one another at the $> 95\%$ confidence level. No one group is responsible for this difference (*e.g.*, removing NGC 3557, the marginally X-ray-detected group, does not affect the outcome). This result suggests that the BGG, dwarf, and giant populations occupy different orbits (*i.e.*, have not mixed completely).

Figure 7b suggests that the 49 galaxies with significant [OII] emission tend to lie outside the group core and to have larger peculiar velocities than the quiescent galaxies. In fact, the overall R distribution in Figure 7b differs from that in Figure 7a at the $> 95\%$ level. As in the case of the quiescent galaxies, the R distributions for the 36 emission line dwarfs and 12 emission line giants are significantly different (at the $> 95\%$ level). The R values for the dwarfs are typically smaller (also as in Figure 7a), implying that the star forming dwarfs are more concentrated radially and/or in velocity space than the star forming giants.

To examine how D/G varies with radius, and thus with mass density, we focus on the larger sample of quiescent galaxies. Figure 8 shows D/G in three radial bins for the quiescent galaxies of each group in Figure 7a. A Spearman rank-order test yields a strong correlation coefficient of -0.62 , which is significant at the $> 95\%$ level. (The middle point for HCG 42 is not plotted, because the group has no giant members within this annulus. However, if we assume conservatively that the missing point has the highest rank D/G in the sample, the Spearman coefficient is still significant at the $> 95\%$ level.) The trend is likely to be even steeper than shown in Figure 8, because the sample includes two Hickson Compact Groups, which have unusually low core D/G values (the two lowest filled circles in the first bin) due to Hickson's (1982) selection criteria. Removing the marginally X-ray detected group NGC 3557 (open circles), which is sampled only to $0.4h^{-1}$ Mpc and has the lowest $D/G_{0.4}$, increases the steepness of the trend and the significance of the Spearman correlation coefficient.

⁴The BGG of NGC 4325 is star forming, and the BGG of HCG 62 is fainter than M_R^* .

The results of this section show that the dwarf and giant populations are not well-mixed and that D/G decreases with radius, and therefore increases with mass density, within the group environment. Mass segregation, in which bright galaxies are brought via dynamical friction into the group core, would produce the opposite trend. However, mass segregation might lead to mergers with the BGG that would disguise its effects. While these results do not include evidence for mass segregation, there are implications for models of standard biased galaxy formation that we discuss in the next section.

4. Discussion

Our results suggest that dwarf-to-giant ratio increases with the mass density of the environment. This trend exists among poor groups, from the field to groups and rich clusters (at least up to the densities of X-ray luminous poor groups), and within the groups themselves. How might we explain the dependence of D/G on environment, an effect that runs counter to the prediction of standard biased galaxy formation? Empirically, we know that there is some relationship between a galaxy’s morphology and the density of its environment (Dressler 1980). It is also observed that the surface density of dwarfs projected within $\sim 250h^{-1}$ kpc of giant ellipticals is at least $3\times$ that around giant spirals (Lorrimer *et al.* 1994). Therefore, the combination of these two effects alone would lead us to expect a boost in D/G with environmental density.

While a morphology-density relation may be a natural consequence of standard biased galaxy formation (*i.e.*, the most massive galaxies, giant ellipticals, form preferentially in the dense environments of clusters), the relative excess of dwarfs around giant ellipticals is not. The latter effect may instead be due to an environmental variation in the efficiency of galaxy formation or in the frequency of galaxy-galaxy mergers. To date, there are few detailed theoretical models of such environmental/morphological influences on D/G . Scenarios that increase D/G include: 1) giant galaxies form less efficiently in denser environments (cf. David & Blumenthal 1992), and dwarfs are the leftover material, 2) cold HI clumps (*e.g.*, the High Velocity Clouds in the Local Group (Blitz *et al.* 1998)) are more likely to collide, produce stars, and evolve into dwarfs in denser regions, 3) galaxy mergers, which occur more frequently in dense systems, reduce the giant population and transfer both progenitors’ satellites to a single remnant, 4) galaxy mergers produce tidal tails in which additional dwarfs form (Barnes & Hernquist 1992; Hunsberger *et al.* 1996), and 5) dynamical friction in denser environments increases the merger rate of giants with the central, giant elliptical, which then acquires their satellites. Although it is not possible to distinguish among these possibilities at present, we note that the non-mixing of the BGG, dwarf, and giant populations, in addition to the clustering of dwarfs about the central BGG, suggests that at least one of these populations evolved later than the

others.

There is preliminary evidence that D/G has evolved in other nearby environments. For example, in the simple environments of isolated, giant elliptical galaxies (cf. Mulchaey & Zabludoff 1999; Colbert, Mulchaey, & Zabludoff 1999), we have found indications of mergers. The giant elliptical NGC 1132 has a poor group-like X-ray halo and dwarf population, yet there are no other giant galaxies in its field. This result is consistent with the picture that NGC 1132 is a merged group.

The consistency of the dwarf-to-giant ratio for the clusters in Trentham’s (1997) and Driver *et al.* ’s (1998) samples with that of the X-ray luminous groups is reminiscent of another surprise in the comparison of groups and rich clusters. Zabludoff & Mulchaey (1998) find that some X-ray groups have early type galaxy fractions similar to those of clusters, despite the lower velocity dispersions of the groups. The strong correlation between velocity dispersion and early type fraction in groups thus deviates from linearity at cluster velocity dispersions. This saturation point occurs at a velocity dispersion of 400-500 km s^{−1}, the value that a poor group would require to enable an M^* galaxy member to experience a merger within a Hubble time. Therefore, it is possible that mergers cause some evolution in the early type fraction of poor groups and cease to be effective in richer groups and clusters. The apparent saturation of dwarf-to-giant ratio with system density observed here may be a manifestation of the same phenomenon.

The results of this paper are inconsistent with the prediction of standard biased galaxy formation models, in which galaxy formation is modulated coherently over scales larger than the galaxy correlation length, and further motivate “local biasing” models (cf. Narayanan *et al.* 1998), in which the efficiency of galaxy formation is determined by the density, geometry, or velocity dispersion of the local mass distribution.

5. Conclusions

We use multi-object spectroscopy and wide-field CCD imaging to examine the shape of the galaxy luminosity function (GLF) in six poor groups of galaxies. Five of these groups have luminous X-ray halos and thus represent an environment in which the GLF has never been isolated. For these five groups, the composite group GLF for galaxies with $-23 + 5\log h < M_R < -16 + 5\log h$ and within projected radii of $\lesssim 0.4 - 0.6h^{-1}$ Mpc from the group center is consistent with a Schechter function with $M_R^* = -21.6 \pm 0.4 + 5\log h$ and $\alpha = -1.3 \pm 0.1$.

Our other conclusions are:

1. *The GLF is not universal in poor groups.* The ratio of dwarfs ($-17 + 5\log h \geq M_R > -19 + 5\log h$) to giants ($M_R \leq -19 + 5\log h$) is significantly larger for the five luminous X-ray groups than for the one marginally X-ray detected group. The difference between the X-ray properties of NGC 3557 and the X-ray luminous groups

may reflect a difference in their potential well depths, as only deep wells heat gas to X-ray-detectable levels (cf. ZM98, MZ98). Because all of the groups have roughly the same physical scale, this result suggests that D/G increases with mass density for these systems.

2. *The dwarf-to-giant ratios of X-ray luminous groups are consistent with or smaller than those for rich clusters.* The composite GLF for the luminous X-ray groups is consistent in shape over the full magnitude range with two measures of the composite GLF for rich clusters (Trentham 1997; Driver *et al.* 1998) and flatter at the faint end than another ($\alpha \approx -1.5$, Smith *et al.* 1997). This result suggests that *if* there is any shape difference between the poor group and rich cluster GLF’s, it arises from a larger dwarf-to-giant ratio in the denser cluster environment.

3. *Dwarf-to-giant ratios are larger in X-ray luminous groups than in regions outside of groups and in poorer groups.* The shapes of our composite group GLF and the large volume, R-band, Las Campanas Redshift Survey field GLF (Lin *et al.* 1996) differ at the $> 95\%$ level. The shape difference is due either to an excess of dwarfs, a deficiency of giants, or a combination of both effects in poor X-ray groups. Because the LCRS is dominated by galaxies in environments more rarefied than those of these groups, this result suggests that D/G increases with mass density from the field to X-ray luminous groups.

4. *Quiescent galaxies cause most of the difference between the dwarf-to-giant ratios of X-ray luminous groups and the field.* The GLF for emission line galaxies (EW [OII] $> 5 \text{ \AA}$) in the X-ray groups is indistinguishable from that of the LCRS field. On the other hand, the GLF’s for non-emission line galaxies in the groups and in the field differ at the $> 95\%$ level. Thus, the shape difference between the overall field and group GLF’s (and presumably between the field and rich cluster GLF’s) is due mostly to the population of quiescent galaxies, whose D/G is larger in the denser group environment than in the field (cf. Ferguson & Sandage 1991, Bromley *et al.* 1998).

5. *Quiescent dwarfs are more concentrated about the group center than quiescent giants, except for the central, brightest ($M_R < M_R^*$) elliptical.* A comparison of the velocities and projected positions of the brightest group galaxies (BGG’s), giants, and dwarfs in the X-ray groups suggests that these populations occupy different orbits (*i.e.*, have not mixed completely) and may have evolved via different mechanisms and at different times. Furthermore, the group D/G decreases with radius and therefore increases with mass density.

Our results show that the shape of the GLF varies with environment and that this variation is due primarily to an increase in the dwarf-to-giant ratio of quiescent galaxies in higher density regions, at least up to the densities characteristic of X-ray luminous poor groups. This behavior suggests that, at least in some environments, dwarfs are more biased than giants with respect to dark matter. This trend is in conflict with the prediction of standard biased galaxy formation models. If more than

standard biased formation is at work, then possible explanations include inefficient galaxy formation (*e.g.*, giants form less efficiently in denser environments), increases in the satellite-to-primary ratio through the mergers of giant galaxies, and dwarf formation in the tidal tails of giant merger remnants (cf. Hunsberger *et al.* 1996).

We thank the referee, John Huchra, for his careful reading of the manuscript. We thank Dennis Zaritsky for his comments on the text and for helpful suggestions. We also thank Huan Lin and Michael Vogeley for providing software used in some of our analyses, Neil Trentham and Huan Lin for providing electronic copies of their data tables and for useful discussions, and Romeel Davé, Simon Driver, Neal Katz, Joel Primack, Ian Smail, David Spergel, and Scott Trager for important information. This paper is based on observations made at Las Campanas Observatory, Chile. AIZ acknowledges support from NSF grant AST-95-29259 and NASA grant HF-01087.01-96A. JM acknowledges support provided by NASA grant NAG 5-2831 and NAG 5-3529.

Table 2: Group Properties

Group	α			δ			N_{grp}^a	\bar{v}^a	σ_r^a	$\log L_X^b$	r_{samp}	N'_{grp}^c	$n_{0.4}$	$D/G_{0.4}$
	2000.0							km s ⁻¹		h^{-2} erg s ⁻¹	h^{-1} Mpc		h^3 Mpc ⁻³	
NGC 2563	8	20	23.4	+21	08	59	44	4775 ± 65	$419 + 56, - 50$	42.0	0.61	44	115.8	2.9 ± 1.2
HCG 42	10	00	07.2	-19	40	17	35	3830 ± 47	$266 + 37, - 32$	42.1	0.49	34^d	68.7	2.1 ± 1.0
NGC 4325	12	23	21.4	+10	37	48	26	7614 ± 68	$328 + 54, - 47$	42.6	0.60	25	67.5	3.5 ± 2.0
HCG 62	12	53	12.4	-09	12	12	63	4356 ± 50	$390 + 37, - 34$	42.3	0.56	63	85.2	0.9 ± 0.4
NGC 5129	13	24	28.1	+13	55	32	38	6998 ± 51	$304 + 41, - 36$	42.2	0.60	32	94.8	1.5 ± 0.7
NGC 3557 ^e	11	09	58.5	-37	23	03	22	2843 ± 64	$282 + 50, - 43$	40.4	0.37	22	37.3	0.2 ± 0.2

^a calculated within r_{samp} except for NGC 4325 (within $1.0h^{-1}$ Mpc) and NGC 5129 (within $0.9h^{-1}$ Mpc)

^b from Mulchaey & Zabludoff (1998) except for NGC 3557 (this paper)

^c calculated within r_{samp}

^d $N_{grp} \neq N'_{grp}$ because one member lies outside photometric survey boundary

^e marginally-detected in X-rays

References

- Barnes, J.E. & Hernquist, L. 1992, *ARA & A*, **2**, 705
- Bertin, E. & Arnouts, S. 1996, *A & A*, **117**, 393
- Binggeli, B., Sandage, A., & Tammann, G. 1988, *ARA & A*, **2**, 509
- Blitz, L., Spergel, D., Teuben, P., Hartmann, D., & Burton, W.B. 1998, preprint (astro-ph/9803251)
- Bromley, B., Press, W., Lin, H., Kirshner, R. 1998, *ApJ*, **505**, 25
- Colbert, J., Mulchaey, J., & Zabludoff, A. 1999, in prep.
- David, L. & Blumenthal, G. 1992, *ApJ*, **389**, 510
- Dressler, A. 1980, *ApJ*, **236**, 351
- Driver, S., Couch, S., & Phillipps, S. 1998, *M.N.R.A.S.*, **287**, 415
- Ferguson, H. & Sandage, A. 1991, *AJ*, **101**, 765
- Geller, M., Kurtz, M., Wegner, G., Thorstensen, J., Fabricant, D., Marzke, R., Huchra, J., Schild, R., & Falco, E. 1997, *AJ*, **114**, 2205
- Graham, J. 1982, *PASP*, **94**, 244
- Grebel, E. 1999, in “The Stellar Content of the Local Group”, *IAU Symp. 192*, eds. P. Whitelock & R. Cannon, *ASP Conf. Ser.*
- Helou, G., Madore, G., Schmitz, M., Bica, M., Wu, X. & Bennett, J. 1991, in “Databases and On-Line Data in Astronomy,” ed. D. Egret & M. Albrecht (Dordrecht: Kluwer), p. 89.
- Hickson, P. 1997, *ARA & A*, **2**, 357
- Hickson, P. 1982, *ApJ*, **255**, 382
- Hunsberger, S., Charlton, J., & Zaritsky, D. 1998, *ApJ*, **505**, 536
- Hunsberger, S., Charlton, J., & Zaritsky, D. 1996, *ApJ*, **462**, 50
- James, P. 1991, *M.N.R.A.S.*, **250**, 544
- Jarvis, J.F. & Tyson, J.A. 1981, *AJ*, **86**, 476
- Jerjen, H. & Tammann, G. 1997, *A & A*, **321**, 713
- Kauffmann, G., Nusser, A., & Steinmetz, M. 1997, *M.N.R.A.S.*, **286**, 795
- Koranyi, D., Geller, M., Mohr, J., & Wegner, G. 1998, *AJ*, **116**, 2108
- Kravtsov, A. & Klypin, A. 1999, preprint (astro-ph/9812311)
- Lin, H., Kirshner, R.P., Shectman, S.A., Landy, S.D., Oemler, A., Tucker, D. L., Schechter, P. L. 1996, *ApJ*, **464**, 60
- Lin, H. 1995, Ph.D. Thesis, Harvard University
- López-Cruz, O., Yee, H., Brown, J., Jones, C., & Forman, W. 1997, *ApJL*, **475**, L97

- Lorrimer, S., Frenk, C., Smith, R., White, S., & Zaritsky, D. 1994, *M.N.R.A.S.*, **269**, 696
- Loveday, J., Peterson, B., Efstathiou, G., & Maddox, S.J. 1992, *ApJ*, **390**, 338
- Marzke, R., Geller, M., Huchra, J., & Corwin, H. 1994a, *AJ*, **108**, 2
- Marzke, R., Huchra, J., & Geller, M. 1994b, *ApJ*, **428**, 43
- Mink, D. J. & Wyatt, W. F. 1995, *Astronomical Data Analysis Software and Systems IV*, ASP Conference Series, Vol. 77, 1995, R.A. Shaw, H.E. Payne, and J.J.E. Hayes, eds., p. 496.
- Moore, B., Lake, G., & Katz, N. 1998, *ApJ*, **495**, 139
- Moore, B., Katz, N., Lake, G., Dressler, A., & Oemler, A. 1996, *Nature*, **379**, 613
- Mulchaey, J. S. & Zabludoff, A.I. 1998, *ApJ*, **496**, 73 (MZ98)
- Muriel, H., Valotto, C., & Lambas, D. 1998, *ApJ*, **506**, 540
- Narayanan, V., Berlind, A., Weinberg, D. 1998, preprint (astro-ph/9812002)
- Ramella, M., Geller, M.J., & Huchra, J.P. 1989, *ApJ*, **344**, 57
- Schechter, P.L. 1976, *ApJ*, **203**, 297
- Schild, R. 1977, *AJ*, **82**, 337
- Secker, J. & Harris, W. 1996, *ApJ*, **469**, 623
- Shectman, S.A., Schechter, P.L., Oemler, A.A., Tucker, D., Kirshner, R.P., & Lin, H. 1992, in *Clusters and Superclusters of Galaxies* (ed. Fabian, A.C.) 351-363 (Kluwer, Dordrecht)
- Shectman, S.A., Landy, S.D., Oemler, A., Tucker, D.L., Lin, H., Kirshner, R.P.; Schechter, P.L. 1996, *ApJ*, **470**, 172
- Smith, R., Driver, S., & Phillipps, S. 1997, *M.N.R.A.S.*, **287**, 415
- Thompson, L. & Gregory, L. 1993, *AJ*, **106**, 2197
- Trentham, N. 1997, *M.N.R.A.S.*, **290**, 334
- Tucker, D., Hashimoto, Y., Kirshner, R., Landy, S., Lin, H., Oemler, A., Schechter, P., & Shectman, S. 1998, in *Large Scale Structure: Tracks and Traces*, proceedings of the 12th Potsdam Cosmology Workshop (ed. V. Mueller, S. Gottloeber, J.P. Muecket, J. Wambsganss) 105-106 (World Scientific)
- Valotto, C. A., Nicotra, M. A., Muriel, H., & Lambas, D. G. 1997, *ApJ*, **479**, 90
- White, S., Davis, M., Efstathiou, G., & Frenk, C. 1987, *Nature*, **330**, 451
- Wilson, G., Smail, I., Ellis, R., & Couch, W. 1997, *M.N.R.A.S.*, **284**, 915
- Zabludoff, A.I. & Mulchaey, J.S. 1998, *ApJ*, **496**, 39 (ZM98)
- Zaritsky, D., Zabludoff, A.I., & Willick, J. 1995, *AJ*, **110**, 1602
- Zepf, S., de Carvalho, R., & Ribeiro, A. 1997, *ApJ*, **488**, 11

Figure Captions

Figure 1: Contour map of the diffuse X-ray emission in the NGC 3557 group of galaxies overlaid on the STScI Digital Sky Survey. The X-ray point sources have been removed following the procedure outlined in MZ98. The contours correspond to levels 3, 4, and 5σ above the background. The data have been smoothed with a Gaussian profile of width $30''$. The coordinate axes are J2000.

Figure 2: Galaxy velocity distributions out to 30000 km s^{-1} for the six poor groups in our sample. The shaded histograms indicate the N_{grp} group members identified with the pessimistic 3σ -clipping algorithm described in ZM98. In the group HCG 42, we manually add one galaxy (H42_136; $v = 4587 \text{ km s}^{-1}$) excluded by the membership algorithm to the membership list, because this galaxy’s velocity bin is contiguous with the group’s velocity peak.

Figure 3: Distributions of apparent R magnitudes (m_R) for galaxies with measured velocities in the six poor group fields. The number above each bar indicates the percentage of the total number of galaxies in the field within that magnitude bin represented by the plotted galaxies. Differences between N_{tot} in Figure 2 and N_{spec} here are due to galaxies observed spectroscopically that lie just off the edge of the photometric field. In two groups, NGC 4325 and NGC 5129, our spectroscopy and imaging extend beyond the radius of $0.6h^{-1} \text{ Mpc}$ sampled in the other groups. In these two cases, we also show the m_R distribution for the subset of galaxies within $0.6h^{-1} \text{ Mpc}$ that is used for all subsequent analyses in this paper (shaded).

Figure 4: Galaxy luminosity distributions for the members of each of the six groups in the sample. The first five groups, HCG 42, HCG 62, NGC 2563, NGC 4325, and NGC 5129 are X-ray luminous, whereas the last group, NGC 3557, is only marginally X-ray detected. The total number of spectroscopically-confirmed group members is N'_{grp} . The absolute magnitudes M_R are extinction-corrected and calculated assuming a $H_0 = 100 \text{ km s}^{-1} \text{ Mpc}^{-1}$, $q_0 = 0.5$ cosmology. The shaded boxes are the observed number of group members within that magnitude bin. The solid boxes are the completeness-corrected galaxy counts (§3.1). (For HCG 62, NGC 4325, and NGC 3557, the corrected counts exceed the limit of the y-axis at the faintest magnitudes.)

Figure 5: (a) Top panel: Comparison of the galaxy luminosity function for the composite of the five X-ray luminous groups (filled triangles) and for two composites of nearby rich clusters of galaxies (short dashed line, Trentham 1997; dot-dashed line, Driver *et al.* 1998). To simplify the comparison of the GLF shapes, the curves in panels (a) and (b) are normalized to have the same total number of $M_R \leq -17 + 5\log h$ galaxies as HCG 42. The composite group GLF is derived from averaging the completeness-corrected counts in Figure 4 after normalizing the individual group GLF’s to the same total number of $M_R \leq -17 + 5\log h$ galaxies as HCG 42. The best fit to the group GLF is consistent with a Schechter function with $M_R^* = -21.6 \pm 0.4 + 5\log$

h and $\alpha = -1.3 \pm 0.1$ (thick solid line in both panels). The three composite GLF's are indistinguishable for the given errors. (b) Bottom panel: Comparison of the group GLF in (a) with that of the Campanas Redshift Survey (LCRS) field (long dashed line; Lin *et al.* 1996) to the completeness limit of the LCRS ($M_R \sim -17.5 + 5 \log h$). The LCRS and composite group GLF's differ at the $> 95\%$ confidence level for any choice of relative normalization. A flat faint end slope of $\alpha = -1$ is also plotted for comparison.

Figure 6: Comparison of the GLF for star forming and for quiescent galaxies in X-ray groups and in the LCRS field. The composite group GLF in Figure 5 is split here into (1) the GLF for galaxies whose spectra have $[\text{OII}] \text{ EW} \geq 5 \text{ \AA}$ (open triangles) and (2) the GLF for galaxies with $[\text{OII}] \text{ EW} < 5 \text{ \AA}$ (filled circles). The GLF for the LCRS field is split similarly into star forming (short dashed line) and quiescent (long dashed line) components. Once again each component is arbitrarily normalized to the to the same total number of $M_R \leq -17 + 5 \log h$ star forming or quiescent galaxies as HCG 42. The thick solid line is as in Figure 5b.

Figure 7: (a) Left panel: Velocity offset vs. projected radial offset of 123 quiescent group members from the group centroid for the six groups in the sample. The velocity offset is normalized with the group velocity dispersion (σ_{grp}). The six asterisks are four of the brightest group galaxies (BGGs) and two other galaxies with $M_R < M_R^*$. The open circles are the 56 giants defined by $M_R^* \leq M_R \leq -19 + 5 \log h$. The filled circles are the 61 dwarfs defined by $-19 + 5 \log h < M_R \leq -17 + 5 \log h$. (Note that the data extend to a projected radius of $\gtrsim 0.6h^{-1} \text{ Mpc} > r_{samp}$, because the group centroid shown here and the fiber field center are not precisely coincident in some cases.) Right panel: The distribution of R (§3.4), the quadrature sum of the x- and y-axis offsets of each galaxy, for the BGG (heavily shaded), giant (shaded), and dwarf populations (unshaded). The R distributions suggest that the three populations occupy different orbits (*i.e.*, have not mixed completely). (b) The same as in (a) for 49 star forming group members.

Figure 8: D/G profile for the quiescent members of each group in Figure 7a. The significance of the correlation as determined from a Spearman rank-order test is $> 95\%$. The trend is likely to be even steeper than shown, because the sample includes two Hickson Compact Groups, which have unusually low core D/G values (the two lowest filled circles in the first bin) due to the Hickson Group selection criteria. Removing the marginally X-ray detected group NGC 3557 (open circles), which is sampled only to $0.4h^{-1} \text{ Mpc}$ and has the lowest $D/G_{0.4}$, increases the steepness of the trend and the significance of the Spearman correlation coefficient.

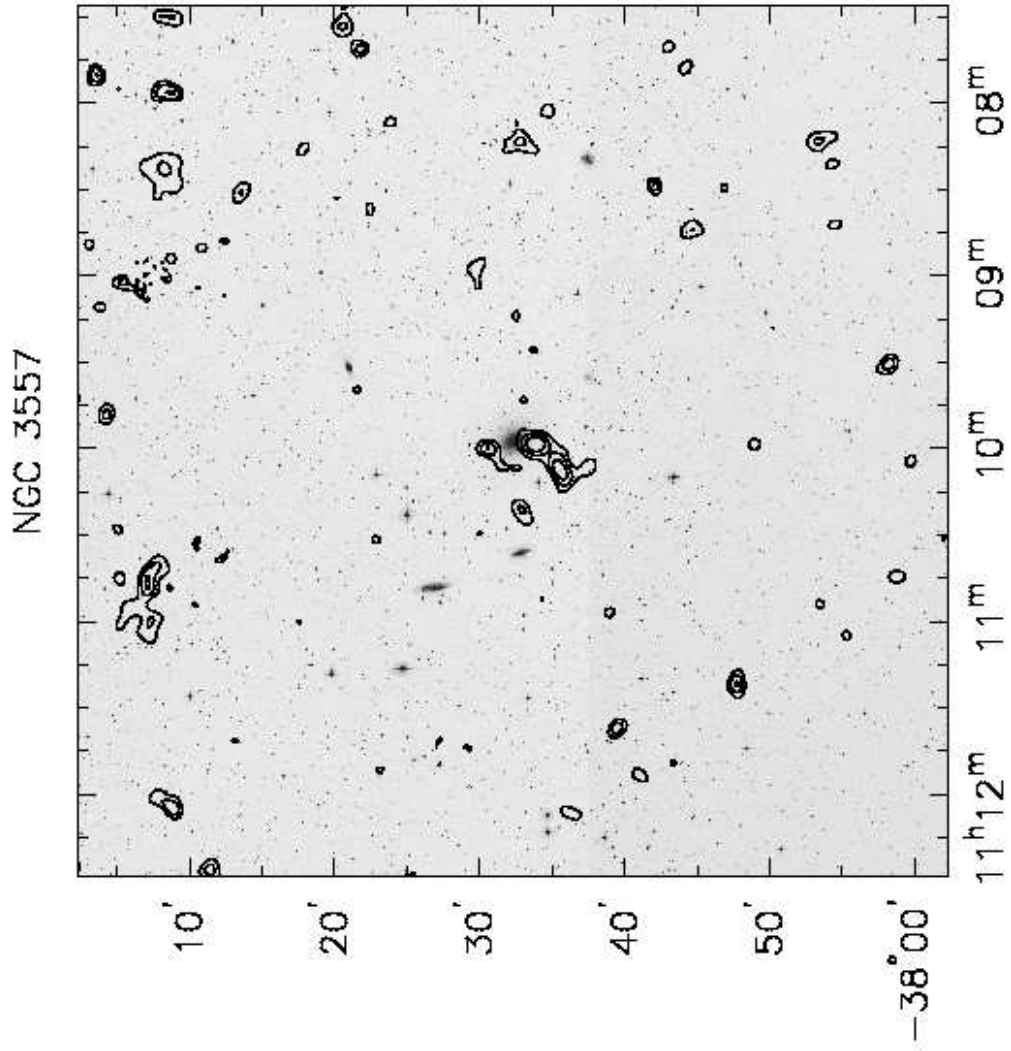


Fig. 1.—

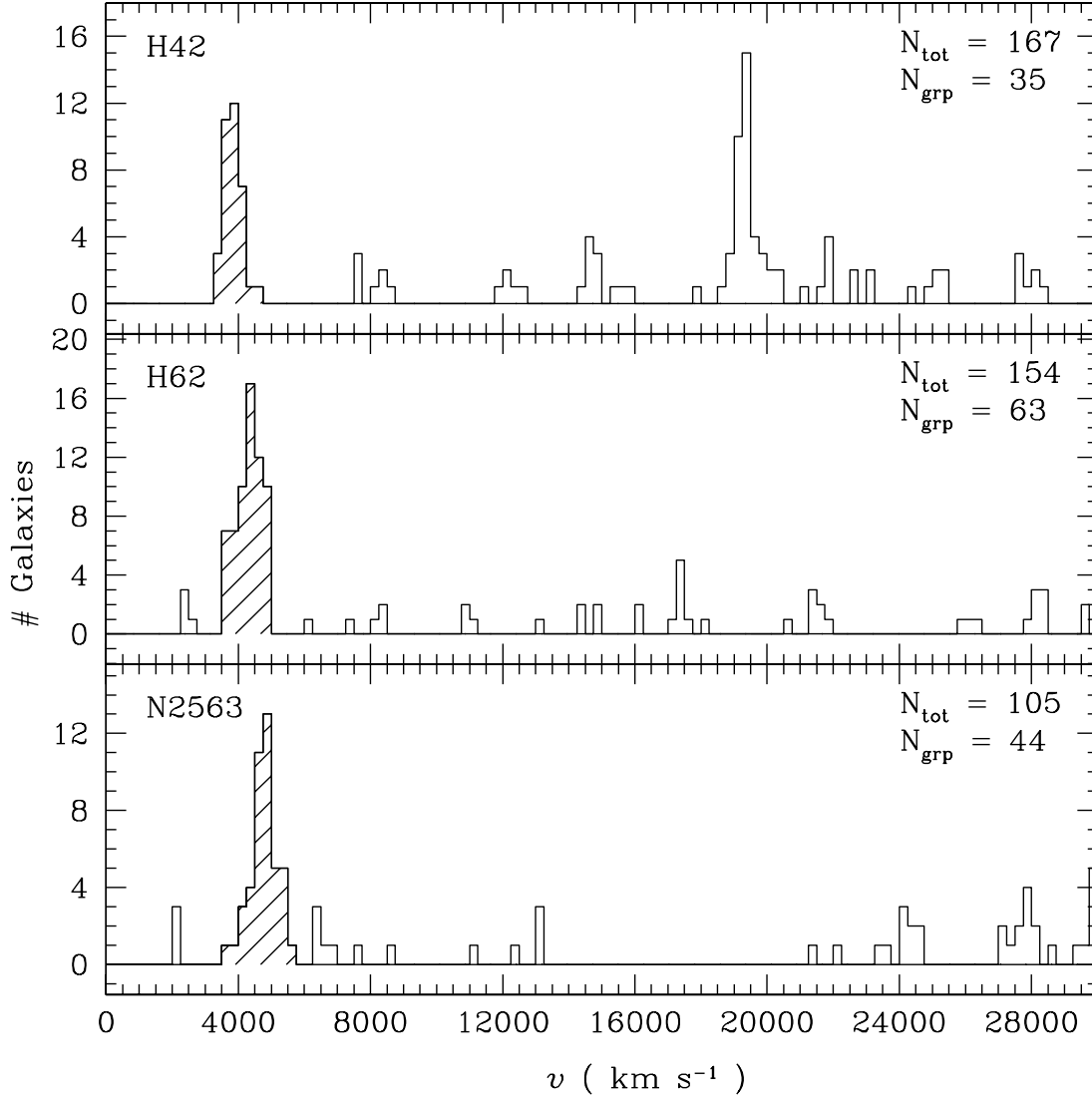


Fig. 2.—

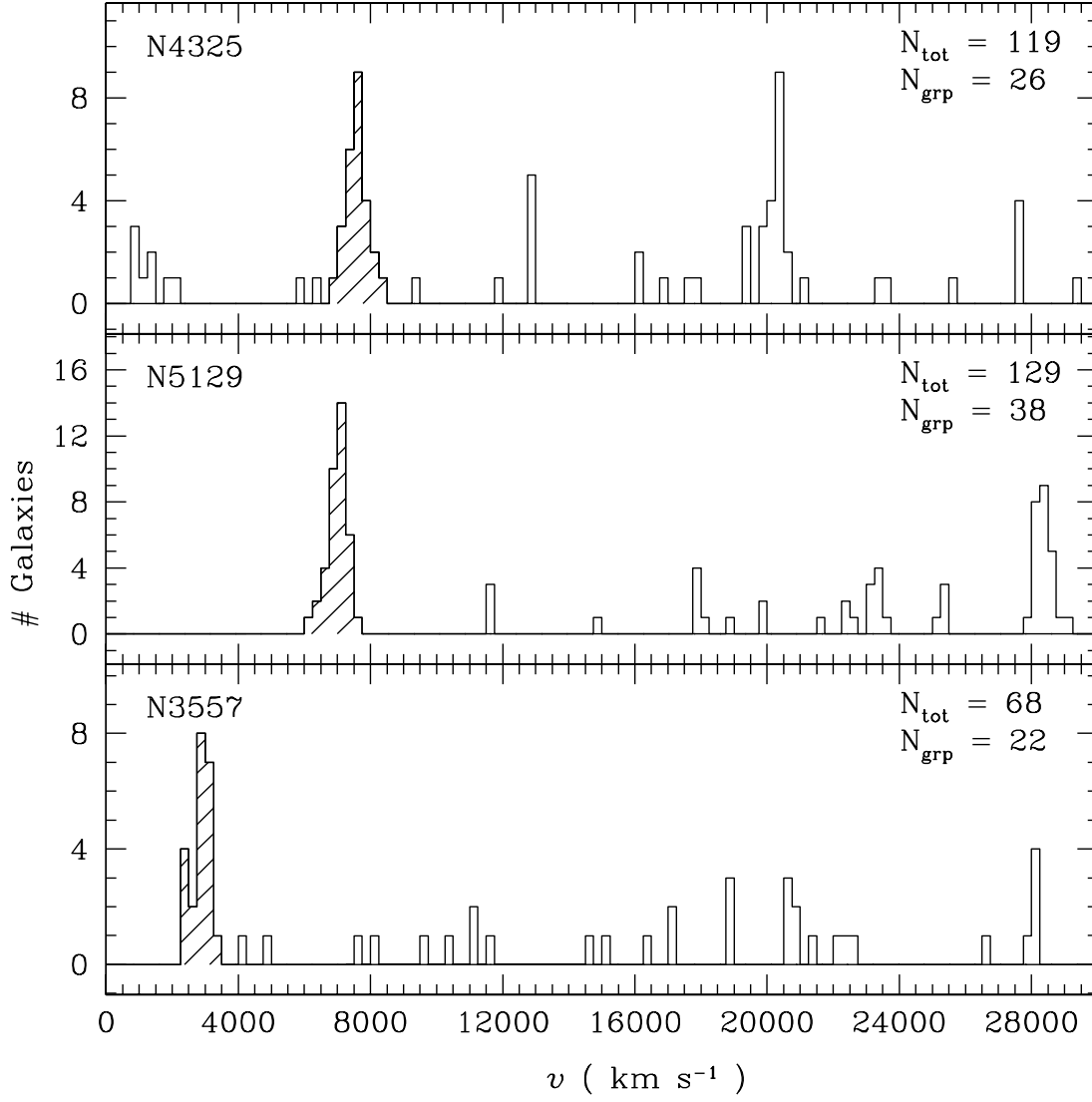


Fig. 2.— *cont.*

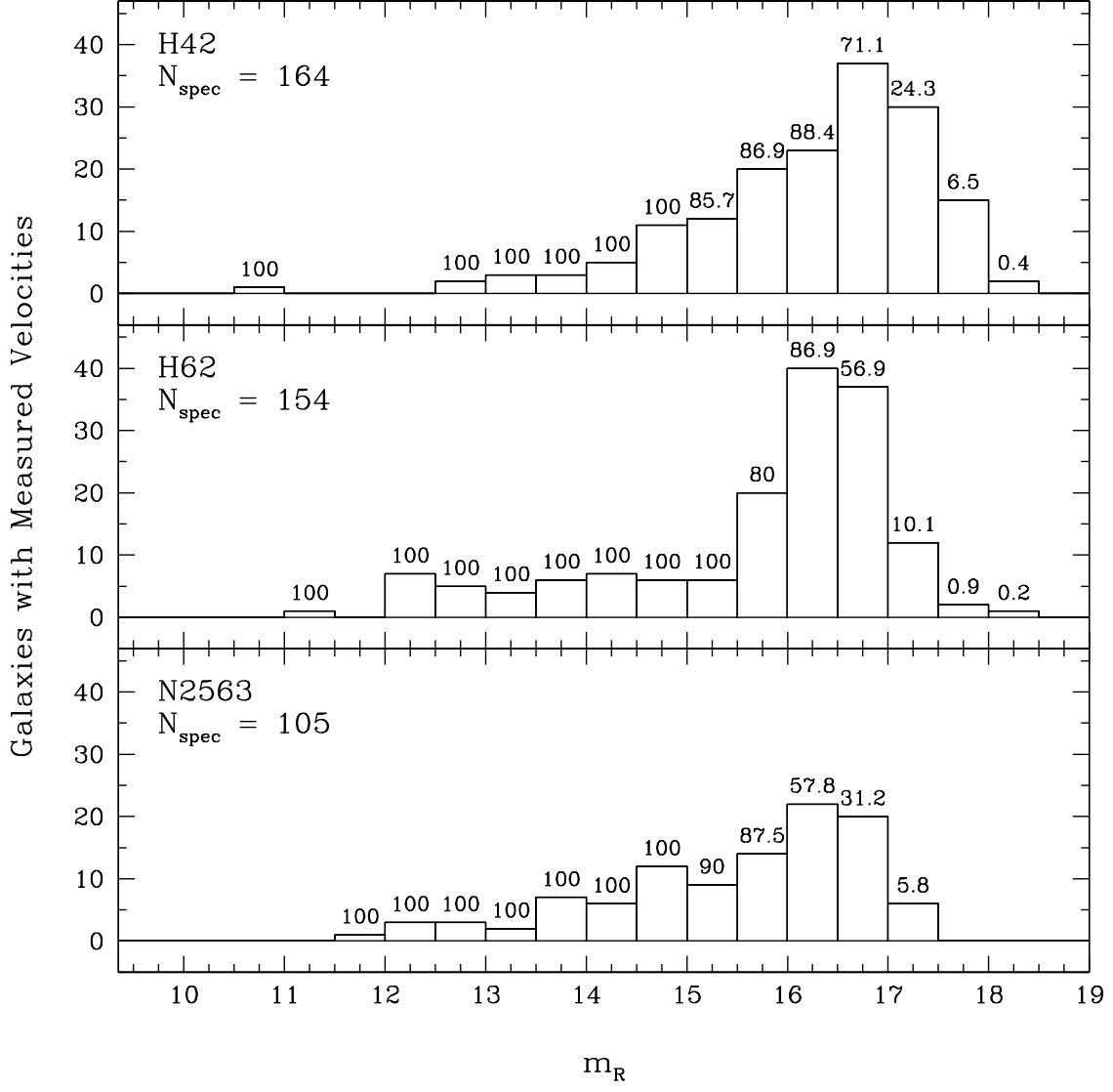


Fig. 3.—

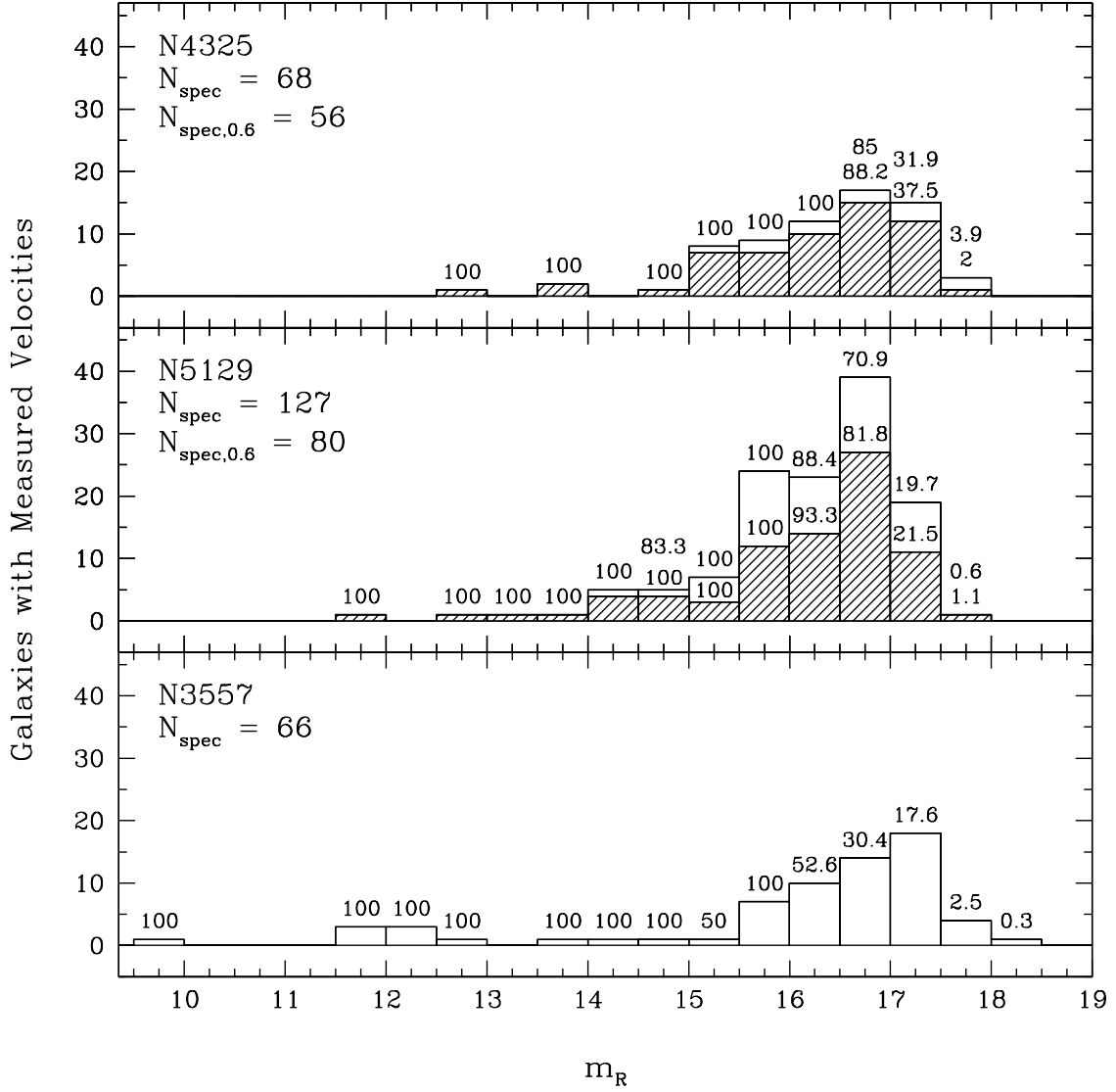


Fig. 3.— *cont.*

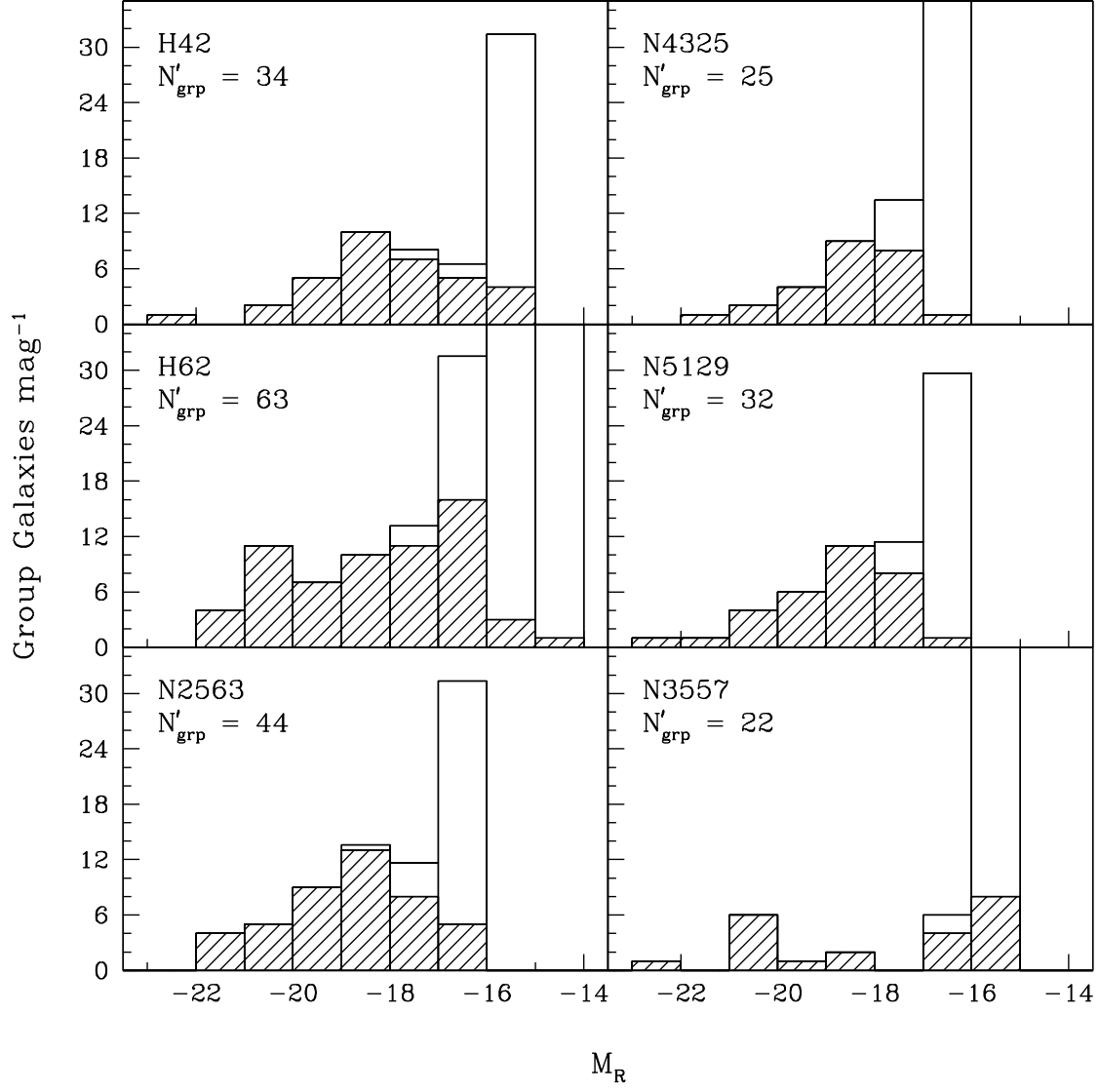


Fig. 4.—

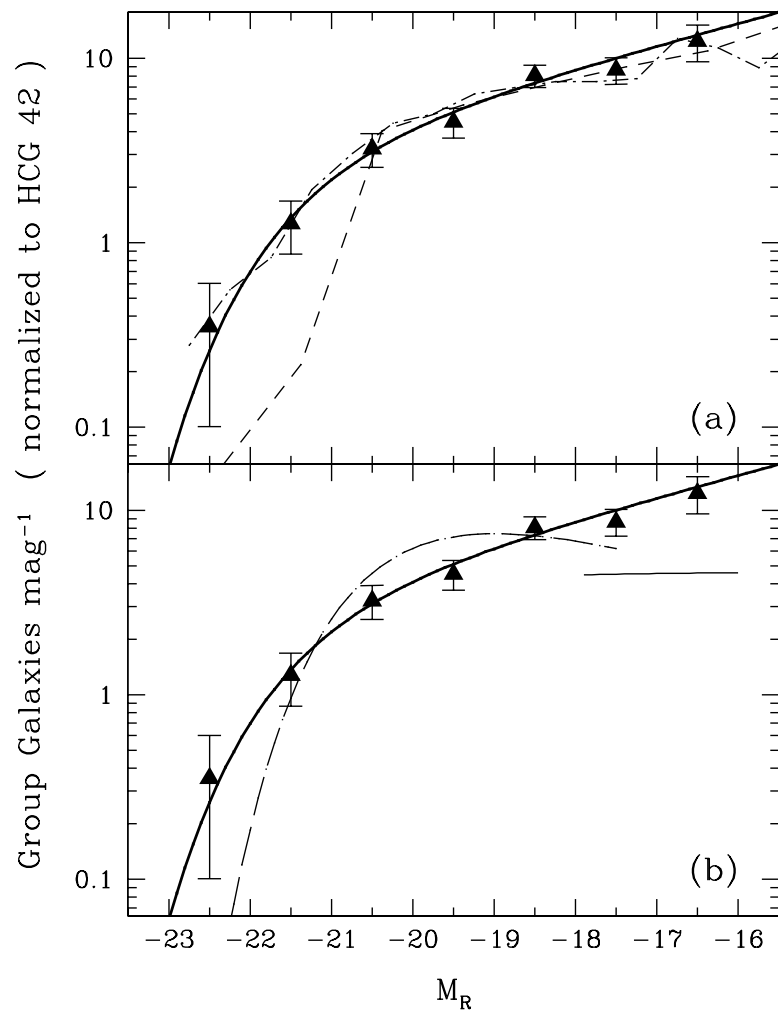


Fig. 5.—

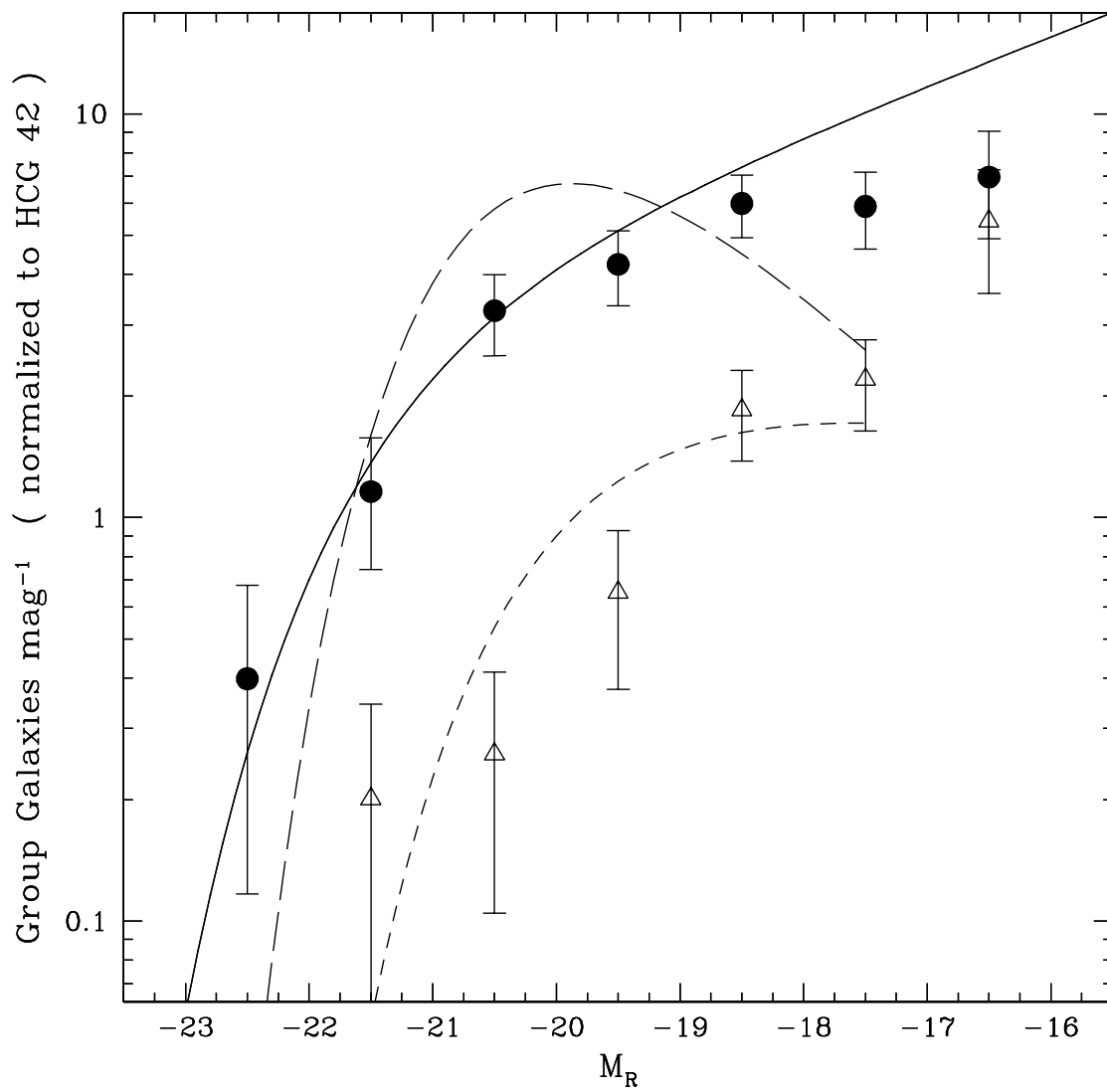


Fig. 6.—

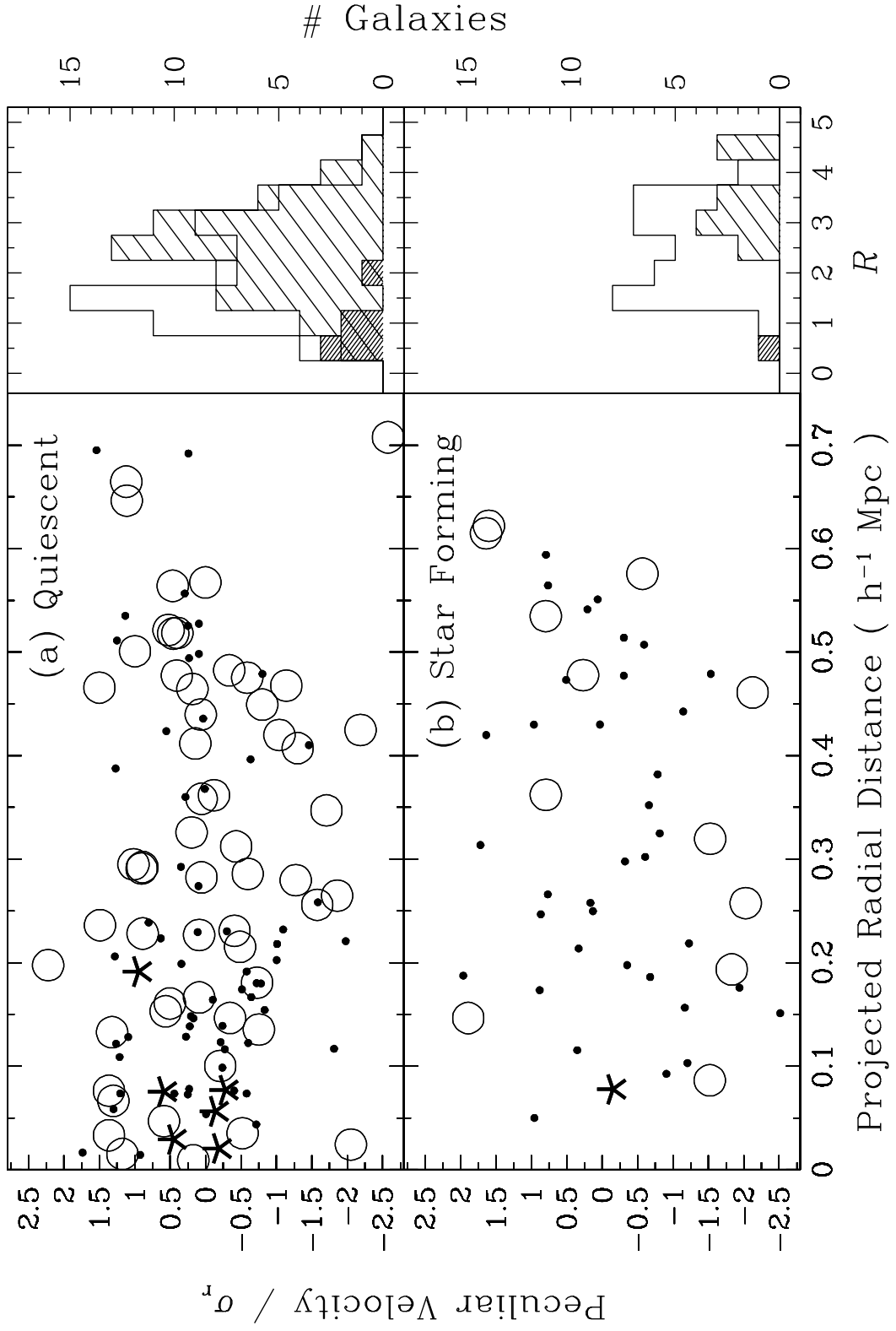


Fig. 7.—

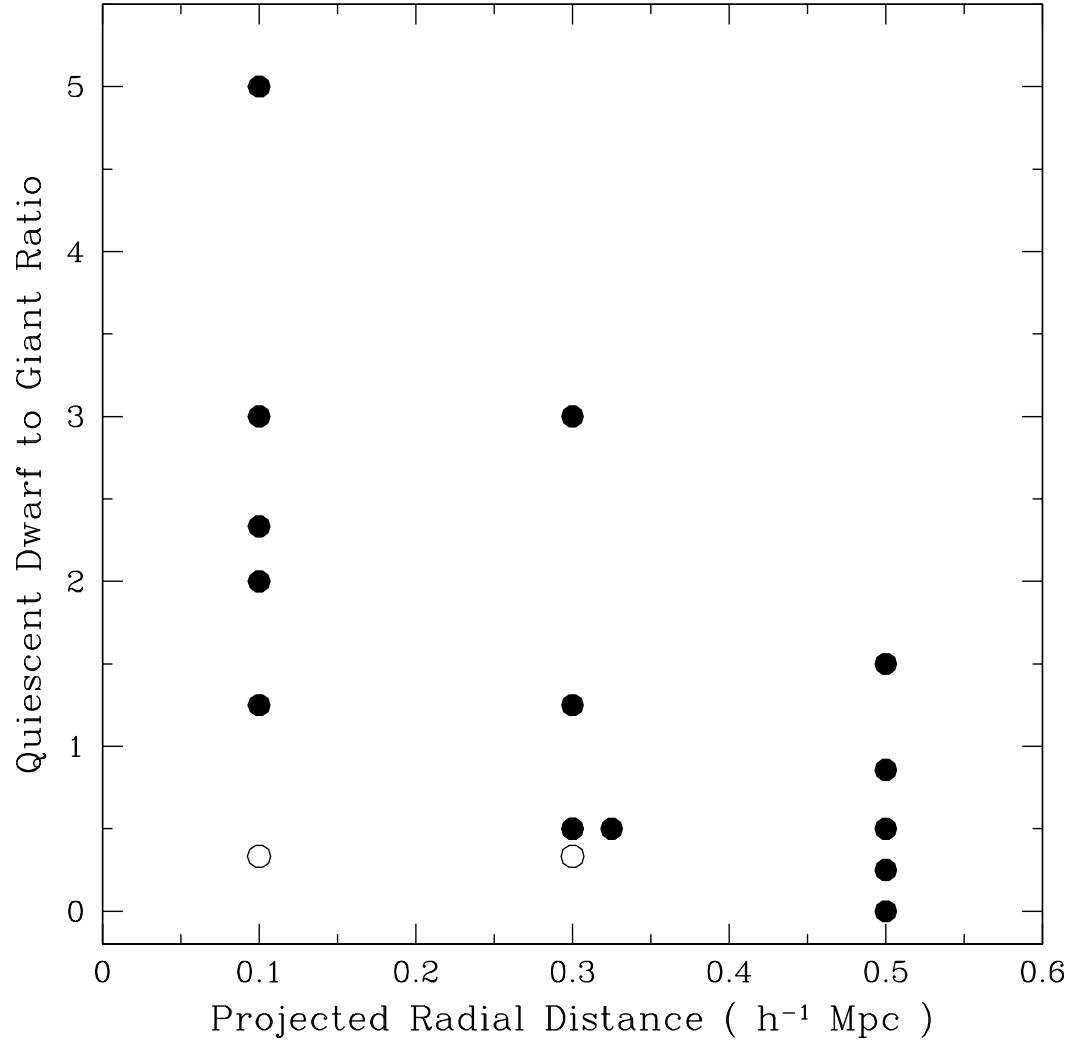


Fig. 8.—

N2563_25	8	17	25.4	21	9	49	2191	80	1	14.8
N2563_2	8	17	25.8	21	41	9	3696	115	0	12.2
N2563_52	8	17	26.7	21	45	24	12274	80	2	15.5
N2563_39	8	17	28.0	21	10	53	2209	80	1	15.3
N2563_155	8	17	31.6	21	0	31	70789	98	0	16.3
N2563_137	8	17	32.4	20	52	33	13032	80	2	16.7
N2563_6	8	17	35.0	20	54	12	4776	80	0	12.7
N2563_69	8	17	38.7	21	42	25	33383	89	0	16.2
N2563_159	8	17	40.5	20	53	33	35077	80	1	17.3
N2563_144	8	17	42.9	21	14	17	29968	80	1	17.0
N2563_31	8	17	52.4	21	6	38	11164	103	0	14.9
N2563_117	8	17	57.8	21	43	59	33476	80	0	16.6
N2563_106	8	17	58.0	21	8	25	8595	80	2	16.4
N2563_141	8	18	10.0	20	51	51	29938	80	2	16.9
N2563_26	8	18	25.7	20	47	16	4987	80	0	14.7
N2563_14	8	18	29.5	20	45	41	4888	80	0	13.8
N2563_9302	8	18	34.8	20	40	13	21404	80	2	16.5
N2563_23	8	18	49.1	21	13	6	4520	80	1	14.5
N2563_32	8	18	50.7	21	2	50	22019	80	0	15.1
N2563_21	8	19	0.8	20	56	14	4594	80	0	14.0
N2563_9	8	19	1.9	21	11	8	4110	80	1	14.6
N2563_123	8	19	3.1	20	40	27	23523	80	2	16.6
N2563_98	8	19	4.0	20	50	1	29487	80	0	16.3
N2563_11	8	19	5.0	21	47	30	4536	80	2	13.7
N2563_94	8	19	5.4	21	14	48	4844	80	1	16.5
N2563_57	8	19	5.8	21	9	2	24007	80	0	15.8
N2563_3	8	19	10.7	21	26	9	4857	80	0	12.6
N2563_4	8	19	12.7	20	30	38	4969	80	0	12.5
N2563_28	8	19	13.0	20	45	28	5307	80	0	14.7
N2563_24	8	19	19.8	21	3	32	4914	80	1	14.5
N2563_97	8	19	22.9	21	2	51	28189	80	0	16.3
N2563_38	8	19	24.3	21	0	13	3945	80	0	15.1
N2563_75	8	19	25.0	21	43	47	27949	80	0	16.2
N2563_18	8	19	32.0	21	23	40	4114	80	2	14.1
N2563_92	8	19	36.0	21	14	29	4504	80	0	16.0
N2563_10	8	19	37.8	21	6	52	5567	80	1	13.4
N2563_43	8	19	38.0	21	17	7	4473	80	0	15.2
N2563_53	8	19	38.8	21	3	53	4286	80	2	15.7
N2563_127	8	19	41.3	21	20	12	24663	80	1	16.7
N2563_84	8	19	42.9	20	58	39	28508	80	0	15.7
N2563_42	8	19	43.5	21	2	13	28087	80	0	15.0
N2563_88	8	19	48.3	21	14	10	2058	80	1	16.2
N2563_157	8	19	49.8	20	50	16	66549	80	0	17.0
N2563_136	8	19	50.5	21	34	0	34085	123	0	16.7
N2563_5	8	19	51.8	20	59	6	4812	80	0	12.7
N2563_102	8	19	55.5	21	22	35	34531	80	0	16.5
N2563_33	8	19	58.8	21	3	58	4270	80	1	15.3
N2563_153	8	20	1.9	21	0	42	24672	80	2	17.0
N2563_85	8	20	3.0	21	37	32	33901	80	0	16.0
N2563_110	8	20	4.9	20	35	14	23425	80	0	16.7
N2563_56	8	20	8.5	20	44	23	24481	83	0	15.8
N2563_119	8	20	10.4	21	18	29	34356	94	0	16.7
N2563_16	8	20	10.9	21	4	9	5346	80	0	14.1
N2563_133	8	20	11.4	21	12	10	24221	116	0	16.9
N2563_101	8	20	12.8	21	39	45	34429	80	0	16.2
N2563_27	8	20	16.7	20	52	31	5040	80	2	14.7
N2563_46	8	20	17.2	20	50	32	13149	111	0	15.3
N2563_87	8	20	18.0	20	40	28	24465	80	0	16.3
N2563_86	8	20	20.3	21	6	22	6932	80	2	16.3
N2563_107	8	20	20.9	20	26	41	36298	80	0	16.6
N2563_160	8	20	21.0	21	31	14	34143	80	0	16.9

N2563_8	8	20	23.6	21	7	51	5267	80	0	12.5
N2563_78	8	20	25.4	21	48	26	34222	80	0	16.1
N2563_105	8	20	25.5	21	20	2	30905	80	0	16.5
N2563_77	8	20	27.9	21	10	57	29942	80	0	16.3
N2563_147	8	20	29.3	21	44	16	7705	80	1	16.6
N2563_68	8	20	32.0	21	43	13	13020	80	2	16.1
N2563_72	8	20	34.0	21	7	36	29874	80	0	15.9
N2563_82	8	20	34.5	21	6	20	5176	110	0	16.2
N2563_1	8	20	35.8	21	4	4	4658	80	0	11.7
N2563_51	8	20	39.5	21	4	46	4606	80	0	15.5
N2563_62	8	20	42.5	20	57	15	34463	80	2	15.9
N2563_114	8	20	44.2	21	7	47	5076	87	0	16.6
N2563_146	8	20	45.0	21	10	56	29855	80	0	17.1
N2563_148	8	20	50.7	21	13	29	4055	80	0	16.8
N2563_34	8	20	51.2	21	3	18	4661	80	0	14.7
N2563_30	8	20	58.5	21	15	12	4674	80	0	14.5
N2563_58	8	21	7.0	21	10	17	4868	80	0	15.8
N2563_112	8	21	8.8	21	17	32	49434	93	0	16.4
N2563_59	8	21	10.8	21	24	6	24062	80	2	15.8
N2563_44	8	21	15.7	21	26	52	4920	80	0	15.6
N2563_48	8	21	16.0	21	28	12	6488	80	1	15.7
N2563_40	8	21	19.0	21	26	49	4640	80	0	15.2
N2563_13	8	21	21.2	20	52	3	5148	80	0	13.5
N2563_22	8	21	22.6	20	54	38	6482	80	1	14.2
N2563_74	8	21	24.9	20	51	39	29750	80	0	16.1
N2563_41	8	21	26.3	21	7	52	4917	80	0	14.7
N2563_163	8	21	37.2	21	6	58	4375	80	0	17.3
N2563_103	8	21	56.6	20	58	7	27074	92	0	16.4
N2563_111	8	21	59.3	21	13	12	27337	80	1	16.2
N2563_17	8	22	1.4	21	20	34	6387	80	0	14.3
N2563_156	8	22	8.3	21	36	15	27952	80	2	17.1
N2563_15	8	22	16.3	21	5	33	6708	80	0	13.7
N2563_95	8	22	18.9	20	39	56	27930	80	0	16.3
N2563_50	8	22	31.6	20	58	5	4788	80	0	15.6
N2563_120	8	22	35.9	21	27	54	4870	84	0	16.6
N2563_19	8	22	53.1	21	4	41	4529	80	0	13.8
N2563_73	8	22	53.2	20	47	2	27718	80	0	16.0
N2563_150	8	22	56.7	21	20	41	4557	80	1	17.0
N2563_134	8	23	10.4	20	26	28	27060	80	2	17.0
N2563_20	8	23	32.6	21	20	17	5462	80	2	14.3
N2563_12	8	23	34.3	21	20	53	5445	80	1	13.7
N2563_7	8	23	41.4	21	26	6	5244	80	0	13.2
N2563_37	8	23	42.5	21	3	42	27832	80	0	14.9
N2563_55	8	23	47.9	21	2	2	27564	80	0	15.5
H42_41	9	57	16.1	-19	7	56	4020	80	1	...
H42_12	9	57	18.4	-19	13	29	11987	80	0	14.7
H42_9106	9	57	19.5	-19	12	30	12045	80	2	17.8
H42_2	9	57	23.9	-19	21	16	3526	80	0	12.6
H42_145	9	57	24.2	-19	15	20	19474	80	2	17.0
H42_53	9	57	28.0	-19	27	42	24973	80	0	15.7
H42_86	9	57	34.3	-19	29	42	25368	80	2	16.5
H42_151	9	57	36.4	-20	14	59	12020	80	1	...
H42_16	9	57	38.8	-19	30	14	3661	80	2	14.8
H42_155	9	57	41.1	-19	56	30	73535	80	0	...
H42_124	9	57	41.3	-19	50	35	14819	80	2	17.0
H42_105	9	57	47.2	-20	22	48	20473	80	2	17.0
H42_26	9	57	51.8	-19	20	18	3442	80	0	15.5
H42_166	9	57	53.7	-19	3	45	4049	80	1	17.7
H42_37	9	58	5.6	-19	46	30	19272	80	0	15.4
H42_96	9	58	6.2	-19	56	29	19775	80	0	16.2

H42_17	9	58	6.3	-19	13	49	3977	80	0	14.3
H42_35	9	58	10.4	-19	43	3	15994	80	0	15.3
H42_121	9	58	18.8	-20	5	29	15585	80	0	16.7
H42_147	9	58	21.0	-19	20	17	38685	80	2	17.3
H42_143	9	58	23.1	-19	42	19	4081	80	0	17.5
H42_131	9	58	23.2	-19	21	39	7610	80	2	17.2
H42_20	9	58	32.2	-19	21	32	7611	80	1	14.5
H42_177	9	58	38.2	-18	56	25	32878	80	0	17.0
H42_30	9	58	38.7	-19	21	23	7555	80	1	15.9
H42_42	9	58	39.3	-19	53	1	19306	80	0	15.3
H42_54	9	58	42.3	-18	58	27	32906	80	0	15.8
H42_130	9	58	46.3	-20	10	48	43920	80	1	16.9
H42_98	9	58	46.6	-19	58	12	32813	80	1	16.7
H42_183	9	58	50.7	-19	55	54	33348	80	2	17.6
H42_21	9	58	53.1	-19	42	19	3675	80	0	14.3
H42_58	9	58	54.4	-20	12	34	3853	80	2	16.5
H42_135	9	58	56.0	-19	13	55	19412	80	0	17.3
H42_117	9	59	1.3	-20	18	13	28043	80	0	17.2
H42_43	9	59	2.5	-19	44	12	19179	80	2	15.6
H42_172	9	59	7.7	-19	0	31	19176	80	2	17.8
H42_47	9	59	11.0	-20	15	38	28023	80	0	15.6
H42_9977	9	59	13.0	-20	14	0	21080	80	1	17.8
H42_102	9	59	13.9	-18	55	48	35887	100	0	16.9
H42_14	9	59	13.9	-19	51	7	3636	80	0	13.8
H42_109	9	59	16.7	-19	42	44	32705	80	2	17.1
H42_68	9	59	17.6	-19	46	12	19218	80	0	15.7
H42_118	9	59	18.4	-19	2	22	27655	80	2	17.4
H42_28	9	59	18.7	-19	28	22	3621	80	0	14.9
H42_140	9	59	18.8	-19	15	17	56222	80	0	17.0
H42_9459	9	59	22.0	-19	50	25	32795	80	2	17.4
H42_39	9	59	22.1	-20	15	17	14805	80	2	15.2
H42_73	9	59	22.4	-19	17	30	32781	80	1	16.7
H42_107	9	59	22.9	-19	18	5	33116	80	0	16.6
H42_18	9	59	24.4	-20	10	54	14692	80	2	14.8
H42_85	9	59	26.5	-19	38	57	3402	80	2	16.9
H42_45	9	59	27.5	-20	8	23	14677	80	2	15.8
H42_11	9	59	28.4	-19	2	50	14617	80	1	14.7
H42_5	9	59	29.0	-19	29	30	3980	80	0	12.8
H42_76	9	59	30.6	-19	42	13	15468	80	2	16.3
H42_112	9	59	32.2	-19	2	34	14826	80	0	16.4
H42_9500	9	59	34.2	-20	20	29	31795	80	0	17.0
H42_111	9	59	35.1	-19	27	32	19589	80	2	17.3
H42_123	9	59	35.2	-19	31	17	32758	80	0	16.8
H42_72	9	59	36.5	-19	54	44	14333	80	1	16.6
H42_46	9	59	36.9	-19	40	42	3891	80	0	16.0
H42_164	9	59	38.6	-19	24	32	27771	80	0	16.7
H42_25	9	59	39.3	-19	50	30	8425	80	2	15.2
H42_170	9	59	39.4	-19	45	4	12441	80	2	18.0
H42_50	9	59	40.1	-20	16	12	28259	80	0	16.2
H42_116	9	59	44.7	-19	34	56	35930	80	1	16.7
H42_9675	9	59	45.1	-20	13	57	21886	80	2	17.4
H42_62	9	59	45.2	-19	50	50	25214	80	0	16.1
H42_138	9	59	53.1	-19	28	17	36129	80	2	17.8
H42_141	9	59	56.8	-19	4	38	19232	80	0	16.7
H42_38	9	59	57.9	-19	29	16	19808	80	0	15.2
H42_66	9	59	58.0	-19	13	8	19328	80	0	15.6
H42_175	9	59	59.7	-20	23	10	27526	80	2	18.0
H42_146	10	0	0.4	-19	31	14	59688	80	0	16.8
H42_9261	10	0	2.0	-19	52	47	25069	100	0	17.5
H42_136	10	0	3.5	-19	38	24	4587	80	2	17.5
H42_115	10	0	5.8	-19	22	33	19034	80	0	16.5

H42_7	10	0	10.3	-19	37	19	4193	80	0	13.3
H42_24	10	0	12.8	-19	40	20	4076	80	4	14.7
H42_44	10	0	13.5	-20	20	26	21886	80	0	16.1
H42_60	10	0	13.6	-19	0	54	8516	80	2	16.8
H42_1	10	0	14.2	-19	38	9	3950	80	0	10.6
H42_63	10	0	17.4	-19	4	19	19205	86	0	15.9
H42_74	10	0	17.7	-19	3	52	19497	80	0	16.1
H42_171	10	0	17.9	-20	20	38	36169	80	1	17.7
H42_137	10	0	19.6	-20	23	16	20398	80	1	17.6
H42_188	10	0	20.5	-20	5	35	38270	80	0	17.4
H42_56	10	0	23.9	-19	23	0	32666	80	0	15.6
H42_69	10	0	25.0	-19	34	59	3675	80	0	16.0
H42_165	10	0	25.2	-19	17	33	18922	107	0	17.3
H42_22	10	0	28.2	-19	40	15	3828	80	0	14.9
H42_122	10	0	28.3	-20	4	34	38057	80	0	17.0
H42_92	10	0	28.9	-19	41	13	19233	80	1	17.2
H42_139	10	0	29.9	-20	8	53	33385	80	0	17.0
H42_174	10	0	30.1	-19	3	17	19750	80	0	17.1
H42_9	10	0	31.5	-19	11	30	3424	80	1	13.9
H42_93	10	0	31.9	-18	59	0	19654	80	0	16.3
H42_4	10	0	33.0	-19	39	42	4176	80	0	13.0
H42_186	10	0	36.9	-19	10	30	61144	80	0	17.0
H42_59	10	0	37.7	-19	32	54	3647	80	0	16.6
H42_29	10	0	38.1	-19	45	40	3766	80	0	15.2
H42_114	10	0	41.6	-19	18	47	32882	80	0	16.9
H42_3	10	0	43.3	-20	22	3	3879	80	0	13.1
H42_36	10	0	44.2	-19	7	43	18735	80	0	15.0
H42_128	10	0	47.7	-19	19	12	33641	80	0	16.7
H42_77	10	0	47.7	-19	1	31	19377	80	0	16.1
H42_134	10	0	55.0	-19	7	11	44095	80	0	17.0
H42_75	10	0	57.0	-18	58	2	19326	80	2	16.6
H42_52	10	0	58.4	-19	2	57	19510	80	0	15.6
H42_34	10	1	0.3	-19	45	12	3876	80	0	15.4
H42_48	10	1	1.2	-19	2	50	18831	80	0	15.8
H42_10	10	1	3.1	-19	3	29	19322	80	0	13.7
H42_100	10	1	3.9	-18	57	22	23004	80	0	16.2
H42_78	10	1	5.7	-19	1	49	19386	80	0	16.4
H42_89	10	1	7.3	-19	2	19	18906	80	0	15.8
H42_113	10	1	8.4	-19	32	21	33974	80	2	17.2
H42_13	10	1	9.1	-19	26	29	3504	80	1	14.1
H42_9305	10	1	9.4	-19	0	34	12509	80	1	17.4
H42_82	10	1	11.4	-18	57	1	23139	80	0	16.2
H42_83	10	1	15.3	-19	4	48	19348	80	0	15.9
H42_91	10	1	16.1	-19	4	3	19136	80	0	16.1
H42_181	10	1	18.0	-19	23	40	60705	80	2	17.7
H42_9511	10	1	19.7	-19	0	8	19166	80	0	16.8
H42_64	10	1	20.4	-19	2	26	20020	80	0	15.8
H42_127	10	1	23.8	-19	48	36	44123	80	1	17.0
H42_152	10	1	25.0	-20	9	46	21773	80	1	17.4
H42_71	10	1	27.1	-19	3	4	19337	80	0	16.0
H42_6	10	1	31.2	-19	32	22	3538	80	0	14.0
H42_23	10	1	31.4	-20	2	34	3613	80	2	14.8
H42_19	10	1	32.4	-20	23	0	3748	80	2	15.1
H42_178	10	1	32.8	-20	4	8	46045	80	2	16.9
H42_169	10	1	35.2	-19	25	35	45524	81	0	17.4
H42_162	10	1	36.1	-20	7	6	14514	80	2	18.1
H42_157	10	1	36.4	-19	44	38	44334	80	0	17.0
H42_153	10	1	39.8	-18	55	5	27710	80	2	17.3
H42_9425	10	1	42.3	-19	34	9	66342	80	2	17.5
H42_142	10	1	46.7	-19	24	46	32481	80	2	17.7
H42_108	10	1	47.0	-19	4	44	20163	80	0	16.6

H42_15	10	1	48.3	-19	56	29	4287	80	2	14.8
H42_154	10	1	49.9	-19	56	32	4212	80	1	17.8
H42_65	10	1	55.8	-20	8	5	3938	80	0	16.5
H42_70	10	1	55.8	-19	53	12	21748	80	1	15.8
H42_79	10	2	0.6	-19	2	46	19832	80	0	16.3
H42_110	10	2	2.5	-18	56	22	19465	80	0	16.5
H42_33	10	2	4.8	-18	57	22	3908	80	2	15.9
H42_167	10	2	6.4	-20	17	37	44713	102	0	16.8
H42_49	10	2	7.7	-18	56	19	19374	80	0	16.0
H42_133	10	2	28.3	-19	11	10	22747	80	0	16.3
H42_97	10	2	29.9	-19	56	52	38452	80	0	16.6
H42_9700	10	2	32.1	-19	35	6	35502	80	1	17.1
H42_184	10	2	32.5	-19	58	29	31176	80	2	17.7
H42_9747	10	2	33.4	-19	59	8	31189	80	1	17.0
H42_132	10	2	34.6	-19	10	49	22558	88	0	17.0
H42_163	10	2	35.7	-19	41	8	35786	116	0	17.4
H42_90	10	2	44.5	-19	55	1	24281	80	0	16.5
H42_27	10	2	46.2	-20	3	1	8264	80	0	14.5
H42_67	10	2	52.4	-19	0	40	19260	80	0	15.7
H42_173	10	2	54.1	-19	47	22	25264	80	1	17.3
H42_8	10	2	54.3	-20	3	57	8061	80	2	14.1
H42_57	10	2	54.7	-20	4	52	3846	80	0	16.2
H42_159	10	3	7.1	-19	14	35	45184	80	2	17.0
H42_129	10	3	9.4	-19	56	6	44557	80	2	16.9
H42_9598	10	3	11.2	-19	11	41	17823	80	1	18.0
H42_119	10	3	15.3	-19	35	32	21949	80	2	17.0
H42_61	10	3	16.8	-19	53	35	31188	80	2	16.3
H42_190	10	3	28.8	-20	12	27	44037	80	2	17.9
H42_40	10	3	30.1	-19	14	55	19134	80	0	15.1

N4325_15	12	20	6.4	10	4	30	12999	80	0	...
N4325_25	12	20	16.7	10	39	47	20362	80	0	...
N4325_173	12	20	17.3	11	1	48	43975	80	2	...
N4325_108	12	20	22.1	11	9	9	31587	80	1	...
N4325_42	12	20	28.9	10	7	46	20675	80	0	...
N4325_12	12	20	29.5	10	14	43	9441	80	1	...
N4325_10	12	20	30.1	11	20	28	12844	80	0	...
N4325_14	12	20	31.6	10	7	36	20350	80	0	...
N4325_142	12	20	38.3	10	31	59	30678	80	2	...
N4325_104	12	20	46.4	10	40	25	44289	80	2	...
N4325_158	12	20	47.0	10	35	31	30616	80	0	...
N4325_22	12	20	47.0	10	30	42	20197	80	0	...
N4325_146	12	20	47.8	10	18	4	33159	80	2	...
N4325_120	12	20	49.2	11	20	50	45501	80	0	...
N4325_13	12	20	54.6	11	9	43	20660	138	0	...
N4325_9	12	20	55.0	11	0	32	5863	80	0	...
N4325_139	12	20	55.8	10	59	43	23414	80	2	...
N4325_119	12	20	57.8	10	44	48	44166	80	0	...
N4325_157	12	20	58.6	10	55	16	44250	80	0	...
N4325_69	12	21	7.6	11	14	20	35225	100	0	...
N4325_85	12	21	25.7	10	44	22	23554	80	2	16.5
N4325_160	12	21	27.6	10	20	16	40307	80	0	17.4
N4325_126	12	21	34.2	10	2	29	40268	80	2	...
N4325_32	12	21	39.2	10	20	50	20495	80	0	15.8
N4325_8	12	21	45.6	10	35	45	7941	80	0	13.8
N4325_64	12	21	46.3	10	56	20	16243	80	2	16.1
N4325_31	12	21	52.4	10	24	27	20458	80	0	15.6
N4325_16	12	22	2.4	10	37	16	7661	80	2	15.2
N4325_76	12	22	10.5	10	2	48	43024	80	1	...
N4325_81	12	22	13.8	10	34	14	7707	80	0	16.4
N4325_97	12	22	18.1	9	55	46	43907	80	0	...

N4325_27	12	22	18.7	10	2	23	20085	80	1	...
N4325_23	12	22	21.6	10	36	6	2067	104	0	15.1
N4325_137	12	22	30.6	10	23	15	6489	80	2	17.2
N4325_98	12	22	32.4	10	19	25	27687	80	0	16.7
N4325_79	12	22	35.1	10	59	49	7696	116	0	16.4
N4325_91	12	22	37.9	10	6	36	20108	80	1	16.5
N4325_127	12	22	40.2	9	55	18	36906	80	2	...
N4325_111	12	22	43.8	9	54	0	19897	80	1	...
N4325_39	12	22	44.1	10	0	9	20312	80	0	...
N4325_49	12	22	44.6	10	19	19	21080	80	0	16.1
N4325_83	12	22	51.9	10	18	12	7238	80	2	16.6
N4325_166	12	22	52.8	9	58	48	12882	80	1	...
N4325_90	12	22	53.3	11	21	58	41865	80	0	...
N4325_54	12	22	57.0	10	56	52	30807	80	0	16.0
N4325_138	12	22	57.8	10	21	26	20428	80	2	17.0
N4325_53	12	22	57.8	10	8	26	27727	80	0	16.1
N4325_7	12	22	57.8	10	32	55	7779	80	0	13.6
N4325_17	12	22	58.1	10	28	40	7905	80	0	15.2
N4325_89	12	23	0.1	10	40	50	7972	80	0	16.7
N4325_28	12	23	0.3	10	6	5	16211	80	2	15.4
N4325_55	12	23	1.2	10	35	23	7018	80	0	16.2
N4325_145	12	23	4.1	10	25	13	45759	80	2	17.3
N4325_4	12	23	6.6	10	37	17	7564	80	0	12.6
N4325_21	12	23	7.3	10	21	45	20372	80	1	15.3
N4325_50	12	23	9.5	10	32	48	7416	80	0	16.1
N4325_99	12	23	11.0	10	24	18	20370	80	0	16.6
N4325_87	12	23	12.9	10	56	33	41621	80	0	16.5
N4325_37	12	23	14.8	10	30	42	7340	80	0	15.8
N4325_6	12	23	17.1	11	22	4	1434	80	0	...
N4325_122	12	23	19.6	10	48	35	32179	80	0	16.9
N4325_174	12	23	20.5	10	35	4	8146	80	1	17.5
N4325_44	12	23	23.0	10	14	48	20297	80	0	15.8
N4325_150	12	23	23.5	10	17	59	8151	80	1	16.9
N4325_96	12	23	23.6	10	46	29	19425	80	2	16.6
N4325_116	12	23	27.5	10	11	7	48179	80	2	17.1
N4325_140	12	23	27.7	10	55	6	39866	80	0	17.1
N4325_136	12	23	28.3	10	45	54	6978	80	2	16.7
N4325_128	12	23	30.2	10	46	6	41478	116	0	16.9
N4325_30	12	23	31.4	10	41	24	7316	80	1	15.5
N4325_124	12	23	31.8	9	58	20	7490	101	0	...
N4325_156	12	23	34.0	10	34	13	20239	80	2	17.0
N4325_109	12	23	34.4	10	51	31	41987	87	0	16.8
N4325_129	12	23	34.8	10	36	49	7696	80	0	17.2
N4325_165	12	23	35.1	10	23	29	32751	80	0	17.3
N4325_123	12	23	40.3	10	41	46	27717	80	0	16.8
N4325_110	12	23	42.6	9	59	53	12946	80	2	...
N4325_78	12	23	46.3	10	46	43	7650	80	0	16.4
N4325_133	12	23	52.9	10	28	55	7656	80	0	16.8
N4325_132	12	23	53.6	10	19	29	27644	80	2	17.1
N4325_153	12	23	55.3	10	34	49	8256	80	2	17.1
N4325_18	12	23	59.6	11	20	5	19440	80	0	...
N4325_82	12	23	59.6	10	29	15	36313	80	1	16.5
N4325_73	12	24	1.0	10	40	39	39136	80	0	16.4
N4325_159	12	24	2.1	10	28	32	50570	80	0	17.3
N4325_35	12	24	2.8	10	50	56	7397	80	0	15.6
N4325_2	12	24	4.9	11	13	5	1980	80	0	...
N4325_95	12	24	5.2	10	4	4	1370	112	0	...
N4325_147	12	24	8.5	10	22	49	17969	80	2	17.1
N4325_164	12	24	9.3	9	55	48	12980	80	2	...
N4325_106	12	24	10.4	10	42	31	7647	80	0	16.8
N4325_43	12	24	16.5	11	0	45	30723	80	0	16.0

N4325_19	12	24	19.5	10	26	48	17649	80	1	15.5
N4325_52	12	24	23.9	10	16	19	16972	80	2	15.9
N4325_151	12	24	26.1	9	54	30	25560	80	2	...
N4325_60	12	24	34.8	10	53	32	7419	80	2	16.2
N4325_11	12	24	37.5	10	50	21	7747	80	1	14.5
N4325_29	12	24	39.2	10	35	55	7187	80	0	15.4
N4325_68	12	24	48.8	10	3	42	19416	80	0	...
N4325_162	12	24	52.4	10	17	51	40970	80	0	17.3
N4325_141	12	24	59.4	10	29	40	56933	80	0	17.2
N4325_9707	12	25	0.4	10	14	10	30629	150	0	17.9
N4325_47	12	25	4.0	10	6	4	904	80	0	16.0
N4325_172	12	25	18.9	10	7	9	29306	80	1	17.7
N4325_59	12	25	19.3	11	2	58	39503	80	0	16.0
N4325_101	12	25	20.1	11	7	51	50263	80	0	16.8
N4325_1	12	25	22.1	10	1	1	920	80	0	...
N4325_168	12	25	30.3	11	8	13	44219	80	2	...
N4325_38	12	25	35.1	10	28	30	19904	80	0	...
N4325_58	12	25	35.3	10	9	36	30247	80	1	...
N4325_117	12	25	46.6	9	55	21	47638	80	1	...
N4325_3	12	25	50.7	10	27	33	1050	80	0	...
N4325_45	12	25	51.4	10	9	35	19958	80	0	...
N4325_71	12	25	53.3	9	55	20	48194	80	0	...
N4325_148	12	25	53.9	10	51	16	57249	80	0	...
N4325_5	12	25	57.9	10	3	14	922	80	0	...
N4325_56	12	25	58.3	9	56	37	47938	86	0	...
N4325_167	12	25	59.5	10	4	15	48733	80	0	...
N4325_9743	12	26	9.2	10	52	16	11891	80	1	...
H62_118	12	50	10.3	-9	48	19	39211	80	0	16.7
H62_81	12	50	14.2	-8	35	33	14761	80	1	16.0
H62_99	12	50	22.0	-8	39	13	4654	92	0	16.4
H62_104	12	50	28.5	-9	56	44	11186	80	2	16.8
H62_53	12	50	28.5	-8	56	32	14500	80	1	15.9
H62_34	12	50	29.2	-8	58	5	4392	80	0	14.9
H62_80	12	50	31.6	-9	52	7	4956	80	0	16.0
H62_17	12	50	33.4	-9	27	0	4534	80	0	12.2
H62_6	12	50	34.4	-9	27	46	4511	80	0	12.5
H62_20	12	50	34.6	-9	31	11	4666	80	1	14.0
H62_9365	12	50	38.5	-9	43	36	21465	80	0	16.4
H62_7	12	50	39.8	-9	1	50	4225	80	1	13.0
H62_9604	12	50	40.0	-8	34	54	28140	80	0	16.7
H62_15	12	50	42.8	-8	45	53	10973	80	1	13.7
H62_57	12	50	49.9	-9	4	39	2665	80	1	16.4
H62_97	12	50	49.9	-9	9	2	17448	80	0	15.8
H62_136	12	50	52.5	-9	33	8	32123	80	2	17.1
H62_21	12	50	53.3	-9	51	43	4789	80	0	12.6
H62_115	12	50	55.3	-8	37	23	28318	80	1	16.4
H62_88	12	50	58.4	-9	21	50	14471	80	2	16.1
H62_134	12	50	59.5	-9	48	43	39498	80	0	16.3
H62_91	12	50	59.5	-8	54	55	6091	80	2	16.6
H62_149	12	51	1.9	-8	57	5	14808	80	1	17.3
H62_46	12	51	2.3	-8	58	47	4731	80	2	16.2
H62_9301	12	51	12.8	-9	36	26	52352	80	0	16.9
H62_85	12	51	13.6	-9	49	5	39804	80	0	16.1
H62_9356	12	51	18.6	-9	32	45	37661	80	0	16.7
H62_129	12	51	21.5	-9	38	6	26306	106	0	16.8
H62_67	12	51	24.0	-8	42	28	4447	80	2	16.0
H62_16	12	51	24.6	-9	24	28	4310	80	0	13.7
H62_146	12	51	28.2	-9	44	23	17471	80	2	16.8
H62_157	12	51	31.2	-9	56	10	4547	80	2	17.4
H62_131	12	51	31.6	-9	3	38	30141	80	0	16.5

H62_108	12	51	32.9	-9	34	28	30022	80	0	16.5
H62_68	12	51	36.0	-9	37	51	30438	80	0	15.6
H62_9482	12	51	36.9	-9	44	24	39905	80	0	16.4
H62_161	12	51	39.8	-9	25	47	30202	80	0	16.4
H62_94	12	51	42.3	-9	1	9	30043	80	0	16.5
H62_143	12	51	43.9	-9	57	13	2345	80	2	17.1
H62_55	12	51	45.8	-9	9	29	4655	80	0	15.7
H62_42	12	51	48.0	-8	49	52	7341	80	2	15.7
H62_86	12	51	49.0	-8	37	58	8317	80	2	15.9
H62_71	12	51	49.8	-8	46	0	28382	80	1	15.7
H62_139	12	51	52.8	-8	35	12	30466	80	1	16.7
H62_116	12	51	53.5	-9	20	28	30612	80	0	16.3
H62_106	12	51	55.1	-9	24	46	30974	80	0	16.2
H62_60	12	51	55.8	-9	54	30	4322	80	2	16.4
H62_75	12	52	1.5	-9	1	12	4397	119	0	16.3
H62_52	12	52	4.8	-9	53	42	13124	80	0	15.6
H62_25	12	52	5.0	-9	19	58	4391	80	0	14.2
H62_9692	12	52	5.4	-9	27	35	29650	80	0	16.8
H62_72	12	52	6.9	-8	59	49	17584	80	2	16.2
H62_45	12	52	7.1	-9	29	17	30470	80	0	14.6
H62_48	12	52	7.3	-9	19	46	17438	80	0	15.2
H62_9017	12	52	8.0	-9	28	16	30509	80	0	17.0
H62_147	12	52	11.0	-9	10	8	41216	80	2	16.6
H62_9366	12	52	11.7	-8	40	28	41376	80	0	16.7
H62_64	12	52	13.4	-8	32	53	8430	80	1	15.8
H62_9	12	52	13.5	-9	29	51	4378	80	0	13.1
H62_51	12	52	19.1	-9	44	36	17418	80	0	15.0
H62_47	12	52	25.2	-9	49	11	4043	80	0	15.5
H62_9049	12	52	26.1	-9	32	6	73793	90	0	17.0
H62_122	12	52	26.6	-9	42	9	30052	80	0	16.2
H62_24	12	52	27.2	-9	45	10	2266	80	2	13.3
H62_142	12	52	32.1	-9	22	15	21306	80	0	16.4
H62_43	12	52	32.6	-8	59	4	3964	80	0	15.1
H62_103	12	52	33.1	-9	44	13	39914	80	1	16.7
H62_11	12	52	34.7	-9	46	35	2462	80	1	13.0
H62_135	12	52	35.9	-9	35	5	30198	80	0	16.5
H62_76	12	52	40.9	-9	35	14	4963	80	2	16.7
H62_89	12	52	42.1	-9	22	48	4208	80	0	16.4
H62_41	12	52	45.1	-8	59	53	4700	80	1	15.8
H62_36	12	52	45.9	-9	18	6	4829	80	0	14.9
H62_66	12	52	48.7	-9	13	22	4826	80	0	15.9
H62_9975	12	52	48.7	-9	30	32	32114	80	1	17.5
H62_79	12	52	51.4	-9	51	54	28218	80	0	15.6
H62_29	12	52	52.5	-9	30	11	4238	80	0	14.4
H62_125	12	52	54.0	-9	53	17	17140	80	2	17.1
H62_39	12	52	55.2	-9	24	48	4316	80	0	15.3
H62_162	12	52	56.8	-9	22	43	26232	80	2	17.0
H62_152	12	52	57.9	-9	45	58	42385	86	0	16.1
H62_107	12	53	1.4	-9	2	55	39750	105	0	16.5
H62_4	12	53	4.4	-9	11	59	3555	80	0	13.0
H62_1	12	53	5.6	-9	12	13	4284	80	0	11.5
H62_151	12	53	6.6	-9	51	24	4253	80	0	17.0
H62_33	12	53	6.6	-9	15	26	4076	80	0	14.5
H62_144	12	53	8.2	-9	48	40	16035	80	2	17.0
H62_77	12	53	9.4	-9	18	23	16029	80	0	16.0
H62_18	12	53	9.7	-9	11	51	4424	80	0	12.4
H62_148	12	53	10.3	-9	30	57	32426	80	0	16.4
H62_100	12	53	19.8	-8	58	18	3917	102	0	17.1
H62_112	12	53	27.1	-8	29	57	3993	80	0	16.5
H62_150	12	53	31.3	-9	9	29	4671	124	0	17.0
H62_8	12	53	32.3	-9	32	27	3565	80	1	12.2

H62_130	12	53	34.3	-9	44	53	30221	80	2	16.8
H62_23	12	53	35.9	-8	38	42	3949	80	0	13.6
H62_5	12	53	36.0	-8	38	19	3503	80	0	12.2
H62_9795	12	53	36.7	-9	40	23	28321	80	0	16.9
H62_96	12	53	37.2	-9	10	29	31652	80	0	16.5
H62_27	12	53	38.7	-8	54	41	4196	80	0	14.2
H62_141	12	53	39.0	-9	30	58	3722	80	0	17.0
H62_38	12	53	40.3	-8	55	57	3962	80	0	15.1
H62_56	12	53	41.5	-9	18	57	4849	80	0	15.8
H62_61	12	53	43.5	-9	23	28	4695	80	2	16.4
H62_9726	12	53	45.3	-9	26	24	42071	80	0	16.8
H62_9406	12	53	48.2	-9	24	1	31017	80	0	16.6
H62_31	12	53	50.2	-9	49	53	21425	80	1	14.9
H62_119	12	53	53.7	-9	42	46	42337	80	0	16.6
H62_70	12	53	55.7	-9	51	29	21752	88	0	16.2
H62_19	12	53	55.8	-9	7	7	4221	80	0	13.7
H62_22	12	53	55.9	-9	12	22	4871	80	0	13.8
H62_109	12	53	56.1	-9	14	29	4688	80	2	17.2
H62_3	12	53	58.5	-8	46	31	3690	80	0	12.3
H62_30	12	54	3.0	-8	39	13	4369	80	0	14.6
H62_2	12	54	5.2	-8	37	14	3527	80	0	12.4
H62_155	12	54	7.2	-9	38	14	25856	80	0	16.9
H62_114	12	54	9.8	-9	47	42	29574	80	2	16.7
H62_160	12	54	13.1	-9	19	23	4228	80	0	17.3
H62_117	12	54	15.8	-8	30	2	3705	80	0	16.7
H62_14	12	54	19.8	-9	7	2	4166	80	0	13.1
H62_74	12	54	21.6	-8	49	25	20564	82	0	16.0
H62_93	12	54	25.2	-8	52	4	32630	80	0	15.9
H62_49	12	54	37.1	-9	40	31	30553	80	0	15.5
H62_153	12	54	37.3	-8	30	10	35708	80	2	17.1
H62_95	12	54	44.2	-9	45	47	21525	80	2	16.8
H62_123	12	54	48.4	-8	31	18	38067	80	0	16.4
H62_92	12	54	48.9	-9	58	6	31991	80	0	16.5
H62_158	12	54	52.0	-9	43	17	3953	80	0	17.0
H62_113	12	54	55.8	-8	50	19	40591	80	0	16.5
H62_163	12	55	1.5	-9	44	51	30561	80	0	16.5
H62_133	12	55	2.2	-8	51	1	40411	80	0	16.9
H62_110	12	55	6.0	-9	52	7	30313	80	2	16.8
H62_62	12	55	9.2	-9	41	53	4843	80	0	15.9
H62_120	12	55	9.3	-9	45	37	39778	106	2	16.3
H62_10	12	55	9.6	-8	51	30	4382	80	0	12.8
H62_26	12	55	14.1	-8	47	42	3757	80	1	14.3
H62_87	12	55	16.6	-9	21	9	4481	80	0	16.5
H62_124	12	55	24.4	-9	44	19	30297	87	0	16.3
H62_73	12	55	24.6	-8	40	24	18018	80	2	15.7
H62_78	12	55	24.8	-8	54	30	30347	80	2	16.6
H62_32	12	55	28.9	-9	56	0	10854	80	0	14.5
H62_98	12	55	28.9	-9	52	19	21710	80	2	16.5
H62_128	12	55	33.1	-9	29	59	37292	80	2	17.5
H62_28	12	55	36.5	-8	47	32	4798	80	0	14.3
H62_82	12	55	38.7	-9	48	47	4179	80	0	16.7
H62_126	12	55	38.9	-8	53	30	4396	80	1	17.3
H62_12	12	55	42.6	-9	5	25	4940	80	0	13.2
H62_37	12	55	43.9	-8	47	55	4380	80	2	15.6
H62_9354	12	55	46.3	-9	39	28	4621	80	1	18.3
H62_102	12	55	50.5	-9	29	58	27928	80	0	16.1
H62_140	12	55	52.7	-8	53	19	8245	80	2	17.3
H62_84	12	55	53.0	-9	32	44	28074	80	0	16.1
H62_44	12	55	59.1	-8	34	14	4450	80	0	15.1
H62_35	12	55	59.5	-9	36	26	17349	80	0	14.5

N5129_48	13	21	39.3	14	3	59	22584	80	0	...
N5129_24	13	21	44.2	13	23	18	28069	80	0	...
N5129_8	13	21	55.3	14	19	58	7031	80	0	14.4
N5129_45	13	22	2.3	13	22	49	28199	80	0	15.8
N5129_144	13	22	5.2	13	42	13	43745	80	0	16.8
N5129_72	13	22	13.3	14	16	5	17934	80	0	16.2
N5129_95	13	22	17.9	13	58	1	7230	80	1	16.7
N5129_65	13	22	18.6	13	15	54	48234	80	2	16.2
N5129_34	13	22	19.8	13	27	38	27759	80	0	15.7
N5129_150	13	22	24.1	13	28	5	46633	80	2	17.0
N5129_9868	13	22	25.8	13	39	39	19846	80	1	17.0
N5129_19	13	22	26.0	13	22	30	28306	80	0	15.3
N5129_9744	13	22	26.1	13	20	0	28106	80	2	17.3
N5129_138	13	22	38.6	14	11	20	45580	105	0	16.9
N5129_114	13	22	45.6	14	2	39	28293	80	0	16.6
N5129_81	13	22	54.7	13	49	37	28529	80	0	16.3
N5129_9736	13	22	56.5	13	46	47	23099	80	2	17.4
N5129_5	13	23	0.4	13	57	3	7239	80	1	13.8
N5129_100	13	23	4.8	13	49	17	21599	80	0	16.5
N5129_157	13	23	6.1	14	8	20	28520	80	2	17.6
N5129_90	13	23	8.7	13	46	15	28563	80	2	16.6
N5129_146	13	23	8.9	14	5	34	25171	80	2	16.9
N5129_161	13	23	10.8	14	11	0	45418	80	0	16.9
N5129_134	13	23	13.0	13	40	23	28379	86	0	16.9
N5129_131	13	23	17.7	14	7	23	44382	80	0	16.8
N5129_125	13	23	17.9	13	55	24	46927	80	0	16.8
N5129_88	13	23	18.0	13	23	17	28238	80	0	16.4
N5129_43	13	23	25.5	13	34	26	28161	80	0	15.6
N5129_111	13	23	28.6	13	31	24	28063	80	0	16.9
N5129_156	13	23	28.8	13	27	34	47296	85	0	17.4
N5129_9	13	23	30.8	13	46	22	7273	80	0	14.4
N5129_164	13	23	34.5	13	30	46	47249	80	2	17.2
N5129_74	13	23	35.6	13	30	43	28106	80	2	16.4
N5129_10	13	23	36.9	13	58	25	6441	80	1	14.5
N5129_69	13	23	37.2	13	40	0	23428	80	0	16.2
N5129_46	13	23	42.0	13	38	11	28290	80	0	16.0
N5129_9950	13	23	42.4	14	5	48	62663	80	0	17.5
N5129_83	13	23	43.2	14	25	30	7239	82	0	16.2
N5129_140	13	23	46.3	14	17	7	45339	80	0	16.9
N5129_17	13	23	50.0	13	53	44	6768	81	0	15.0
N5129_76	13	23	52.0	14	16	4	25388	80	2	16.4
N5129_6	13	23	52.3	13	44	3	6433	80	0	14.1
N5129_13	13	23	53.5	14	22	17	7157	80	0	14.3
N5129_44	13	23	54.0	14	20	0	6905	80	0	15.7
N5129_107	13	23	54.8	13	52	23	7081	80	0	16.7
N5129_145	13	24	1.7	13	37	2	6760	80	2	17.1
N5129_38	13	24	1.7	13	57	12	7132	80	0	15.8
N5129_39	13	24	7.4	13	58	10	7393	80	0	15.9
N5129_92	13	24	8.6	13	45	12	45323	80	0	16.8
N5129_135	13	24	9.0	13	49	53	45127	80	0	16.9
N5129_116	13	24	9.8	13	50	55	45495	89	0	17.1
N5129_1	13	24	10.0	13	58	36	6956	80	0	11.6
N5129_70	13	24	10.4	13	43	15	44965	80	0	16.2
N5129_122	13	24	10.9	14	3	41	7060	80	0	17.0
N5129_62	13	24	13.7	13	55	47	7526	80	0	15.9
N5129_25	13	24	14.3	13	56	14	17902	80	1	15.5
N5129_58	13	24	14.9	13	46	43	6791	80	0	15.8
N5129_51	13	24	15.1	14	7	55	28492	80	0	15.8
N5129_102	13	24	17.4	14	5	8	6842	80	0	16.7
N5129_130	13	24	21.3	13	15	45	28361	80	0	16.6
N5129_73	13	24	21.5	13	47	41	19820	80	0	16.2

N5129_142	13	24	23.7	14	10	25	28375	80	2	17.2
N5129_7	13	24	24.1	13	56	15	6839	80	0	14.2
N5129_104	13	24	24.3	13	41	13	18027	80	2	16.7
N5129_101	13	24	24.9	13	48	45	6233	80	1	16.5
N5129_84	13	24	28.0	13	41	46	17771	80	1	16.4
N5129_67	13	24	28.4	14	27	43	23222	80	0	15.9
N5129_2	13	24	28.9	14	5	33	7285	80	0	12.6
N5129_21	13	24	31.0	13	28	45	7061	80	2	15.3
N5129_35	13	24	34.8	14	0	11	7105	80	0	15.8
N5129_119	13	24	35.1	13	23	11	28551	80	0	16.8
N5129_77	13	24	37.4	13	14	22	28096	80	0	16.4
N5129_9652	13	24	39.5	13	24	23	47873	80	1	17.1
N5129_159	13	24	43.2	13	45	51	7242	86	0	17.0
N5129_4	13	24	51.4	13	44	16	6817	80	0	13.3
N5129_12	13	24	51.7	13	34	52	6754	80	2	14.6
N5129_11	13	24	52.5	14	4	38	7451	80	0	14.6
N5129_26	13	24	53.1	13	21	50	28318	80	0	15.3
N5129_113	13	24	55.2	13	51	22	7387	80	0	16.9
N5129_61	13	24	55.5	13	52	32	6890	80	0	16.1
N5129_158	13	24	56.7	13	56	59	32355	80	0	17.2
N5129_42	13	24	57.4	13	22	5	28327	80	1	15.7
N5129_137	13	25	0.6	14	7	50	45296	80	2	17.3
N5129_121	13	25	4.5	13	15	2	28516	80	0	16.8
N5129_105	13	25	6.1	14	7	28	44322	80	1	17.3
N5129_127	13	25	7.5	13	24	53	28812	80	0	16.9
N5129_56	13	25	7.8	13	58	33	7261	80	0	16.1
N5129_66	13	25	12.2	13	37	3	23436	80	0	16.1
N5129_15	13	25	14.1	13	34	2	14915	80	0	14.9
N5129_27	13	25	15.5	13	16	33	6549	80	2	15.7
N5129_94	13	25	19.5	13	41	28	29054	80	0	16.5
N5129_148	13	25	23.3	14	20	21	69638	139	0	16.8
N5129_89	13	25	24.6	14	5	51	45194	80	0	16.7
N5129_28	13	25	25.2	13	24	38	22498	80	1	15.8
N5129_91	13	25	25.5	13	25	10	22415	80	2	16.5
N5129_112	13	25	26.0	13	46	33	47829	80	0	16.8
N5129_20	13	25	26.7	13	54	22	25357	80	0	15.4
N5129_108	13	25	27.3	14	2	54	44265	80	0	16.7
N5129_22	13	25	31.7	13	49	11	33076	80	0	16.3
N5129_124	13	25	33.0	14	1	23	32377	80	0	17.0
N5129_30	13	25	36.2	14	12	54	7026	80	0	15.6
N5129_120	13	25	38.9	14	1	47	44538	80	0	16.9
N5129_9899	13	25	46.0	13	54	37	6701	80	2	17.4
N5129_18	13	25	53.5	13	17	53	6653	80	2	15.1
N5129_106	13	25	53.6	13	58	59	32857	80	0	16.7
N5129_9838	13	25	59.8	14	3	31	23409	80	2	17.2
N5129_117	13	26	4.5	13	44	8	11714	80	2	17.1
N5129_71	13	26	7.8	14	10	59	11514	80	1	16.4
N5129_23	13	26	10.9	13	15	45	23382	104	1	15.3
N5129_118	13	26	12.5	13	18	35	45051	80	0	16.8
N5129_64	13	26	14.0	14	15	19	11581	80	2	15.9
N5129_52	13	26	17.3	13	48	37	7058	80	2	15.7
N5129_80	13	26	22.2	14	19	48	33044	80	0	16.2
N5129_16	13	26	32.9	14	25	11	7149	80	2	14.7
N5129_57	13	26	34.5	14	24	34	17802	80	2	15.6
N5129_40	13	26	35.6	13	20	56	44712	85	0	15.8
N5129_141	13	26	38.6	13	20	11	45002	80	0	16.9
N5129_87	13	26	41.6	13	14	31	23557	89	0	16.4
N5129_33	13	26	43.1	13	33	16	23152	80	2	15.7
N5129_149	13	26	46.5	13	31	35	42980	80	0	17.1
N5129_82	13	26	48.8	13	16	56	44404	125	0	16.4
N5129_60	13	26	51.7	14	3	33	44597	93	0	16.0

N5129_63	13	27	0.0	14	2	16	6524	80	2	16.0
N5129_162	13	27	7.1	13	38	56	54246	80	0	16.9
N5129_152	13	27	8.3	13	34	34	42829	80	2	17.1
N5129_86	13	27	8.6	13	59	22	25342	80	0	16.5
N5129_68	13	27	10.9	13	27	58	43110	80	1	16.7
N5129_136	13	27	11.7	13	39	8	44928	80	0	16.8
N5129_126	13	27	14.5	14	5	8	18961	80	2	16.7
N3557_42	11	6	8.4	-37	57	56	20608	80	0	...
N3557_40	11	6	9.9	-37	50	54	22616	80	0	16.4
N3557_63	11	6	13.7	-37	30	51	11635	80	2	17.1
N3557_81	11	6	25.2	-37	12	6	37530	80	0	17.1
N3557_3	11	6	31.7	-37	39	9	2859	80	0	11.9
N3557_23	11	6	31.9	-37	29	52	4155	80	1	16.3
N3557_83	11	6	32.6	-37	42	29	52949	80	2	17.1
N3557_21	11	6	35.0	-37	58	27	7670	80	0	...
N3557_61	11	6	45.2	-38	8	59	20644	80	0	16.3
N3557_108	11	6	48.7	-37	42	28	8190	80	1	17.9
N3557_39	11	7	3.9	-37	27	46	18952	80	0	15.9
N3557_28	11	7	6.2	-38	2	25	18964	80	0	15.3
N3557_2	11	7	7.6	-37	10	24	3130	80	0	12.1
N3557_75	11	7	9.3	-38	6	24	18965	80	1	17.3
N3557_20	11	7	10.4	-37	24	46	4857	80	2	16.2
N3557_43	11	7	16.0	-37	9	36	14740	80	1	16.6
N3557_55	11	7	19.5	-37	20	58	26642	80	2	17.1
N3557_44	11	7	49.0	-37	7	55	21263	80	0	16.1
N3557_56	11	7	50.4	-37	20	0	22166	80	2	16.8
N3557_103	11	7	58.7	-37	16	48	37711	80	0	17.3
N3557_13	11	8	2.6	-37	7	33	20954	80	0	14.9
N3557_109	11	8	6.8	-37	58	30	45556	89	0	17.4
N3557_95	11	8	13.6	-37	50	56	38274	80	2	17.7
N3557_85	11	8	15.7	-37	40	22	17158	80	2	17.5
N3557_84	11	8	16.8	-37	59	10	45530	80	2	17.2
N3557_27	11	8	17.0	-37	21	23	22265	80	0	16.0
N3557_6	11	8	19.8	-37	37	26	3469	80	0	13.0
N3557_31	11	8	27.5	-37	5	8	20787	80	0	15.7
N3557_45	11	8	31.3	-37	15	42	38291	80	0	16.7
N3557_53	11	8	33.3	-38	4	33	16300	80	2	16.9
N3557_58	11	8	40.6	-37	32	11	28074	80	0	16.5
N3557_26	11	8	44.1	-37	24	16	17057	80	1	15.7
N3557_38	11	8	50.2	-37	22	39	3062	80	0	16.6
N3557_34	11	8	51.9	-37	42	4	28061	80	2	15.6
N3557_97	11	9	6.5	-37	13	4	2751	102	0	17.4
N3557_47	11	9	8.4	-37	43	32	3146	80	1	16.6
N3557_16	11	9	10.8	-37	23	59	3183	80	1	15.9
N3557_18	11	9	15.5	-37	55	45	15168	80	2	16.0
N3557_121	11	9	17.2	-37	47	42	38442	80	0	17.5
N3557_25	11	9	21.8	-37	27	48	2772	80	2	16.3
N3557_49	11	9	27.7	-37	38	43	2640	80	0	17.2
N3557_7	11	9	31.4	-37	20	57	3008	80	0	12.1
N3557_60	11	9	33.0	-38	15	42	44252	80	0	16.5
N3557_11	11	9	35.3	-37	37	29	2782	80	0	14.4
N3557_100	11	9	38.9	-36	48	14	20719	80	0	16.8
N3557_36	11	9	40.0	-37	10	13	28209	80	0	16.3
N3557_1	11	9	57.4	-37	32	19	3009	80	0	9.9
N3557_17	11	10	13.6	-37	24	55	2447	80	2	16.5
N3557_66	11	10	18.8	-36	52	47	2388	80	4	16.6
N3557_105	11	10	20.2	-37	1	38	62935	80	2	17.5
N3557_19	11	10	34.8	-38	0	2	3080	80	0	15.5
N3557_9	11	10	36.2	-37	32	51	2784	80	0	11.7
N3557_5	11	10	48.3	-37	26	52	2414	80	2	12.5

N3557_59	11	11	5.3	-36	54	22	11019	80	2	17.0
N3557_88	11	11	15.6	-38	16	28	10324	80	1	17.3
N3557_4	11	11	18.1	-36	52	33	2483	80	0	11.7
N3557_89	11	11	31.1	-38	5	51	55951	80	2	17.3
N3557_32	11	11	42.7	-37	32	10	2623	80	0	16.9
N3557_62	11	11	52.2	-36	59	33	2988	80	2	17.2
N3557_93	11	12	11.5	-37	39	19	27957	80	2	17.6
N3557_52	11	12	11.8	-37	1	50	11042	80	2	16.8
N3557_65	11	12	28.7	-37	42	3	38448	80	0	16.8
N3557_10	11	12	31.2	-36	49	36	2846	80	0	13.7
N3557_79	11	12	51.5	-37	6	17	28050	80	0	16.7
N3557_111	11	13	8.8	-37	50	19	9730	80	1	18.4
N3557_94	11	13	14.3	-37	39	26	37449	114	0	17.1
N3557_99	11	13	14.9	-37	58	6	54001	80	1	17.7
N3557_22	11	13	21.4	-37	8	7	2753	96	0	16.3